

Mössbauer spectrum for diffusing atoms including fluctuating hyperfine interactions

S. Dattagupta*

School of Physics, University of Hyderabad, Hyderabad 500134, India

K. Schroeder

*Institut für Festkörperforschung der Kernforschungsanlage Jülich,
D 5170 Jülich, Federal Republic of Germany*

(Received 9 June 1986)

We present model calculations of Mössbauer emission spectra for mobile substitutional Mössbauer atoms in cubic lattices. The fluctuating hyperfine interactions (isomer shift and quadrupole interaction) due to approaching vacancies are considered. To describe the motion of the Mössbauer atom we use the five-frequency model appropriate for impurity diffusion including binding of Mössbauer atoms and vacancies. For suitable choice of the jump frequencies our model shows the combined effect of quadrupole splitting, motional narrowing, and diffusional broadening of the emitted line. These features have previously been discussed only separately. We present analytical results for diffusion on sc lattices and numerical results for fcc lattices. In particular we find the following. The diffusional broadening of the spectrum is governed by the effective jump frequency of the substitutional Mössbauer atoms which is essentially given by the product of the vacancy concentration and the vacancy-Mössbauer atom exchange jump rate whereas the fluctuation rates of the hyperfine interaction is directly given by the vacancy jump rates (without the factor vacancy concentration). Thus the hyperfine interactions are completely averaged out at temperatures where in normal metals diffusion broadening can be detected. The dynamics of the hyperfine relaxation can only be detected at low temperatures in alloys in which the vacancy concentration is enhanced. Promising systems are nonstoichiometric ordered alloys such as Co-Ga, Pd-Si, Fe-Al.

I. INTRODUCTION

In this paper we study the Mössbauer line shape when the Mössbauer atom (MA) is an impurity in a host cubic crystal. An example is Fe in a single crystal of face-centered-cubic (fcc) Al which will serve as a test case of our theoretical investigation.¹ At finite temperatures the MA is known to diffuse via vacancy-induced jumps. This leads to a broadening of the Mössbauer emission line.²⁻⁵ Two essential features are prominent in the line-shape calculation:⁶⁻⁸ (i) correlation in the MA-vacancy jumps, and (ii) anisotropy of the jump direction with respect to the direction of emission of the γ ray. An additional important aspect, not considered in detail hitherto, is the time fluctuations in the hyperfine interaction of the MA triggered by the approaching vacancy. Here we present a treatment of the combined effects of diffusion and the fluctuating hyperfine interaction on the Mössbauer line shape.

The simplifying assumptions of our model are as follows. (1) The hyperfine interaction, mostly in the form of the isomer shift and electric field gradient, arises only when the vacancy is a nearest neighbor to the MA. (2) The elementary jumps of the vacancy are over nearest-neighbor distances only. (However, for sc and bcc lattices we allow next-nearest-neighbor jumps of the vacancy between the sites of the nearest-neighbor shell of the MA. This permits us to treat fluctuations in the direction of the electric field gradient in these lattices also.) (3) The concentrations of both the impurity (c_i) and the vacancy

(c_v) are low so that only a single impurity-vacancy pair has to be considered at a time. (4) The detailed dynamics of vacancy jumps is treated only for the nearest-neighbor sites of the MA as was first suggested by Krivoglaz and Repetskiy.⁵ Outside of the nearest-neighbor shell we assume an average vacancy occupation. This means we have to treat an effective mobile cluster consisting of the MA and its nearest-neighbor sites embedded in a lattice with an average vacancy occupancy. While assumptions (1)–(3) are reasonable at first sight, (4) needs elaboration. When c_v is small, the probability of finding a vacancy in the nearest-neighbor shell of a MA is small. We can then safely neglect configurations with more than one vacancy in the nearest-neighbor shell. As is well known all jumps of a MA with one particular vacancy are correlated. However, it has been shown⁸ that the major part of the correlation is effected by immediate returns of the vacancy from the nearest-neighbor shell, and vacancy paths beyond the nearest neighbor shell give only small contributions. Thus our approximation of assuming an average vacancy occupation outside the nearest-neighbor shell and neglecting the correlated reentry of the same vacancy is justified. This means that the effective rate of reentry of a vacancy into the nearest neighbor shell is proportional to the average vacancy concentration c_v .

An important ingredient, which distinguishes between impurity diffusion (e.g., Fe in Al) and self-diffusion (e.g., Fe in Fe) is the perturbation of the vacancy jump frequencies in the immediate vicinity of the impurity (i.e., the MA). This is incorporated in our study in terms of the

so-called five-frequency model which was first discussed in the context of tracer-diffusion studies in fcc crystals.⁹ The five frequencies or jump rates, which carry information about the impurity-vacancy binding as well as the potential barriers the vacancy has to jump over, form an essential input of our calculation (see Fig. 2).

The model presented here is similar in spirit to the one discussed earlier by Krivoglaz and Repetskiy.⁵ However, two important generalizations are now introduced: (i) the vacancy jumps *within* the nearest-neighbor shell of the MA, governed by the rate w_1 (see Figs. 1 and 2), are explicitly taken into account, and (ii) time-dependent hyperfine interactions of quantum nature are incorporated. The present analysis therefore goes beyond that of Mantl *et al.*,¹ who considered, within the Krivoglaz-Repetskiy model, classical isomer-shift fluctuations only and treated the $w_1 \rightarrow \infty$ limit.

We should point out that the combined effects of diffusion and a fluctuating hyperfine interaction have been discussed earlier. But these analyses have been restricted to either ideal interstitial diffusion (uncorrelated jumps in an empty lattice¹⁰), or diffusion in a confined region ("cage"¹¹).

An outline of the paper is as follows. In Sec. II we discuss pure diffusional effects within our approximate treatment of the five-frequency model. An analytical expression for the Mössbauer line shape is derived for the simple cubic (sc) structure. This helps illustrate various limiting cases which can be connected with earlier studies of the problem. The analytical results for the sc case serve also as a check on our numerical analysis which is required in other cubic structures (e.g., fcc). In Sec. III we present the main theoretical formulation of the combined occurrence of diffusion and hyperfine interaction. The treatment requires an adaptation of the Blume model¹² in order to incorporate the diffusion effects. The theory is illustrated for the specific case of ⁵⁷Fe atom as the Mössbauer probe. Again, analytic expressions are obtained in the sc case which yield various interesting limits. We present then in Sec. IV numerical plots in the fcc case which should be relevant for Fe diffusion in Al and Cu, for instance. Finally in Sec. V we discuss our main conclusions.

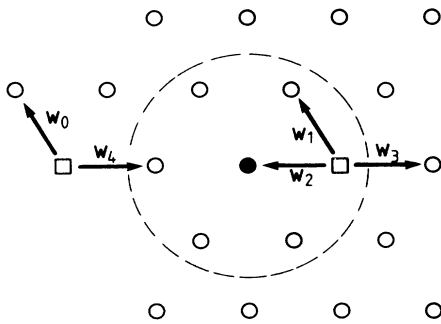


FIG. 1. Kinetic model for the description of impurity diffusion via vacancies (\square). The sphere of influence of the MA (\bullet) extends to the NN shell (encircled). There the vacancy jump frequencies are perturbed (see Fig. 2) and hyperfine interactions are considered (see Fig. 4).

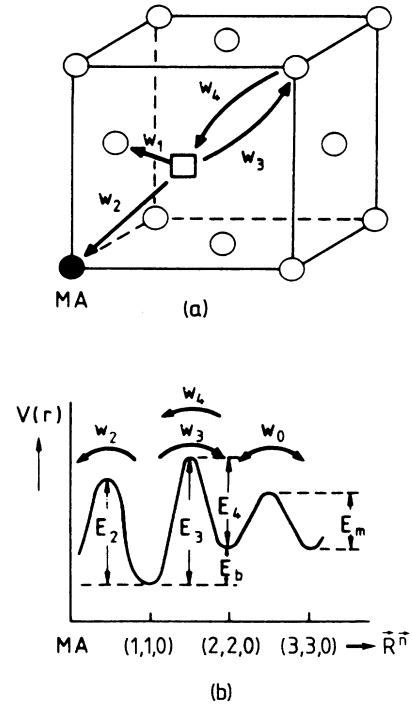


FIG. 2. (a) Five-frequency model for impurity (MA) diffusion in fcc crystals. The vacancy jump frequencies are as follows: w_0 , vacancy jump frequency in the pure host lattice; w_1 , vacancy jump in the NN shell of the MA; w_2 , exchange jump of vacancy with MA; w_3 , dissociation jump of vacancy out of NN shell; w_4 , association jump into the NN shell. (b) Possible energy barriers for vacancy jumps in radial direction. The five frequencies can be parametrized by the corresponding five activation energies (E_1 not shown). $E_b = E_3 - E_4$ is equal to impurity-vacancy binding energy; $E_0 = E_m$ = migration energy in pure host lattice.

II. PURE DIFFUSIONAL EFFECTS

A. Formulation of the problem

The Mössbauer emission line shape can be written as¹

$$\begin{aligned} \sigma_e(\mathbf{k}, \omega) = & f \operatorname{Re} \frac{1}{\pi \hbar} \int_0^\infty dt \exp(-i\omega t - \Gamma_0 t / 2\hbar) \\ & \times \sum_{\mathbf{n}} \exp(i\omega_0 t) \exp(i\mathbf{k} \cdot \mathbf{R}^{\mathbf{n}}) \\ & \times G_D(\mathbf{R}^{\mathbf{n}}, t). \end{aligned} \quad (2.1)$$

Here \mathbf{k} is the wave vector and $\hbar\omega$ the energy of the emitted γ rays, $\hbar\omega_0 = E_e - E_g$ the energy of the nuclear transition, and Γ_0 is the natural linewidth of the excited state of the Mössbauer nucleus. The sum is over all equilibrium sites $\mathbf{R}^{\mathbf{n}}$ of the MA on a discrete lattice and $G_D(\mathbf{R}^{\mathbf{n}}, t)$ is the diffusional part of the self-correlation function. Thus $G_D(\mathbf{R}^{\mathbf{n}}, t)$ measures the conditional probability that the MA is found at $\mathbf{R}^{\mathbf{n}}$ at time t given that it started from the

origin $\mathbf{0}$ at $t=0$. The Debye-Waller factor f describes the reduction of the intensity due to vibrations of the MA on a lattice site. In writing (2.1) we have made the usual assumption that vibrations occur on a much faster time scale than diffusive jumps so that f factors out of the line-shape expression.

The self-correlation function is determined by the kinetics of the MA-vacancy pair. Therefore, referring to Fig. 1 and adopting a matrix notation, we may write

$$G_D(\mathbf{R}^n, t) = \sum_{\alpha, \beta} (\mathbf{R}^n, \alpha | \underline{P}(t) | \mathbf{0}, \beta) p_\beta, \quad (2.2)$$

where $(\mathbf{R}^n, \alpha | \underline{P}(t) | \mathbf{0}, \beta)$ measures the conditional probability that the MA is found at \mathbf{R}^n and the vacancy in the "state" $|\alpha\rangle$ at time t , given that the MA was at the origin $\mathbf{0}$ and the vacancy was in the "state" $|\beta\rangle$ at $t=0$. The state $|\alpha\rangle$ or $|\beta\rangle$, in our model, refers to one of the vacancy sites within the nearest-neighbor shell of the MA (called the "associated" states) or any site (we do not care which one) outside the nearest-neighbor shell (called the "nonassociated" state). Thus the associated states run over Z sites, where Z is the coordination number or the number of nearest neighbors in a lattice ($Z=12$, in the fcc case), while the nonassociated state is just one lumped state. Hence α or β assumes $Z+1$ values. The summations in (2.2) take into account the fact that all final va-

cancy states must be summed over and all initial vacancy states must be averaged over with the aid of p_β , the *a priori* probability of finding the state $|\beta\rangle$.

Our fundamental assumption is that the diffusion of the vacancy within the nearest-neighbor shell as well as in and out of the nearest-neighbor shell may be viewed as a stationary Markov process.¹² Thus the matrix $\underline{P}(t)$ obeys the master equation

$$\frac{\partial}{\partial t} \underline{P}(t) = \underline{W} \underline{P}(t), \quad (2.3)$$

where the elements of the "jump matrix" \underline{W} specify the various allowed jumps for the MA-vacancy pair and the accompanying rates.

In order to illustrate the construction of the jump matrix \underline{W} we consider an sc case for the sake of simplicity (see Fig. 3). Here we have

$$(\mathbf{R}^n, \alpha | \underline{W} | \mathbf{R}^n, \beta) = \delta_{nm} (\alpha | \underline{W}_v | \beta) + (\mathbf{R}^n, \alpha | \underline{W}_{MA-v} | \mathbf{R}^m, \beta). \quad (2.4)$$

The first term in (2.4) describes the situation in which the MA is stationary but the vacancy jumps between the associated and nonassociated states. The corresponding matrix \underline{W}_v , the subscript v specifying vacancy jumps only, can be written as

$$\underline{W}_v = \begin{matrix} & \begin{matrix} 1 & -1 & 2 & -2 & 3 & -3 & N \end{matrix} \\ \begin{matrix} 1 \\ -1 \\ 2 \\ -2 \\ 3 \\ -3 \\ N \end{matrix} & \left[\begin{array}{ccccccc} 1 & -1 & 2 & -2 & 3 & -3 & N \\ -(\nu+4w_1) & 0 & w_1 & w_1 & w_1 & w_1 & \lambda \\ 0 & -(\nu+4w_1) & w_1 & w_1 & w_1 & w_1 & \lambda \\ w_1 & w_1 & -(\nu+4w_1) & 0 & w_1 & w_1 & \lambda \\ w_1 & w_1 & 0 & -(\nu+4w_1) & w_1 & 0 & \lambda \\ w_1 & w_1 & w_1 & w_1 & -(\nu+4w_1) & 0 & \lambda \\ w_1 & w_1 & w_1 & w_1 & 0 & -(\nu+4w_1) & \lambda \\ \nu & \nu & \nu & \nu & \nu & \nu & -6\lambda \end{array} \right] \end{matrix}. \quad (2.5)$$

The diagonal elements of \underline{W}_v contribute to the "loss term" in Eq. (2.3) while the off-diagonal elements contribute to the "gain term." In Eq. (2.5) the first six rows refer to the associated states (since there are six nearest-neighbor sites to the MA atom; see Fig. 3), whereas the seventh row, labeled by N , stands for the nonassociated state. The parameter w_1 describes the rotational jumps of a vacancy in the nearest-neighbor shell of the MA. (Due to the geometry these jumps are next nearest-neighbor jumps in sc and bcc lattices and nearest-neighbor jumps in fcc lattices.) The parameter ν refers to the jump rate out of any associated state and λ designates the jump rate from the nonassociated state to one of the associated states. The parameters ν and λ can be expressed in terms of the elementary jump rates w_3 and w_4 (Fig. 3). For instance, in an sc crystal, five sites outside the nearest-neighbor shell can be reached from any nearest-neighbor site of the MA. Hence,

$$\nu = 5w_3. \quad (2.6)$$

Similarly,

$$\lambda = 5w_4c_v, \quad (2.7)$$

where c_v is the vacancy concentration. We can determine

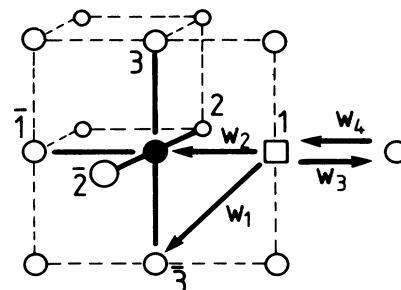


FIG. 3. Enumeration of NN sites of a MA (●) in an sc lattice and vacancy (□) jump frequencies.

also the *a priori* probability p_β from the detailed balance relation

$$p_\beta(\alpha | \underline{W}_v | \beta) = p_\alpha(\beta | \underline{W}_v | \alpha), \quad (2.8)$$

and the probability conservation condition

$$\sum_\beta p_\beta = 1. \quad (2.9)$$

Combining Eqs. (2.8) and (2.9) yields from Eq. (2.5),

$$p_A = \frac{\lambda}{\nu + 6\lambda} = \frac{w_4 c_v}{w_3 + 6w_4 c_v},$$

$$p_N = \frac{\nu}{\nu + 6\lambda} = \frac{w_3}{w_3 + 6w_4 c_v}, \quad (2.10)$$

where p_A refers to the occupational probability of one of the associated states and p_N that of the nonassociated state. Noting that

$$\frac{w_3}{w_4} = \frac{c_v}{c_{NN}} = \exp(-E_b/K_B T), \quad (2.11)$$

where c_{NN} is the nearest-neighbor vacancy concentration and E_b the impurity-vacancy binding energy (cf. Fig. 2), we may reexpress p_A and p_N as

$$p_A = \frac{c_{NN}}{1 + 6c_{NN}},$$

$$p_N = \frac{1}{1 + 6c_{NN}}. \quad (2.12)$$

Equations (2.7) and (2.12) corroborate our earlier remarks in Sec. I in connection with the assumption (4).

Coming back to Eq. (2.4), the second term accounts for MA-vacancy exchanges. From Fig. 3 it is evident that each such exchange will put the vacancy into the opposite associated state. For example, if the vacancy was on state 1 before the exchange, it will be on state -1 after the exchange. Accordingly, the W_{MA-v} matrix can be written as

$$\underline{W}_{MA-v} = \begin{matrix} & \begin{matrix} 1 & -1 & 2 & -2 & 3 & -3 & N \end{matrix} \\ \begin{matrix} 1 \\ -1 \\ 2 \\ -2 \\ 3 \\ -3 \\ N \end{matrix} & \left(\begin{array}{ccccccc} -w_2 \delta_{nm} & w_2 S_{nm} \delta_{nr_1} & 0 & 0 & 0 & 0 & 0 \\ w_2 S_{nm} \delta_{n-r_1} & -w_2 \delta_{nm} & 0 & 0 & 0 & 0 & 0 \\ 0 & 0 & -w_2 \delta_{nm} & w_2 S_{nm} \delta_{nr_2} & 0 & 0 & 0 \\ 0 & 0 & w_2 S_{nm} \delta_{n-r_2} & -w_2 \delta_{nm} & 0 & 0 & 0 \\ 0 & 0 & 0 & 0 & -w_2 \delta_{nm} & w_2 S_{nm} \delta_{nr_3} & 0 \\ 0 & 0 & 0 & 0 & w_2 S_{nm} \delta_{n-r_3} & -w_2 \delta_{nm} & 0 \\ 0 & 0 & 0 & 0 & 0 & 0 & 0 \end{array} \right) \end{matrix}. \quad (2.13)$$

Here the factor S_{nm} ensures that only nearest-neighbor exchanges can take place. Thus

$$S_{nm} = \begin{cases} 1, & \text{if } \mathbf{R}^n \text{ and } \mathbf{R}^m \text{ are nearest neighbors} \\ 0, & \text{otherwise.} \end{cases} \quad (2.14)$$

Further \mathbf{r}_α is the vector joining the MA and the vacancy in the $|\alpha\rangle$ state. This shows explicitly that the transition matrix $(\mathbf{R}^n | \alpha | \underline{W} | \mathbf{R}^m, \beta)$ is a function of $\mathbf{R}^n - \mathbf{R}^m$ only.

From Eq. (2.3) we have

$$\frac{\partial}{\partial t} (\mathbf{R}^n, \alpha | \underline{P}(t) | \mathbf{0}, \beta)$$

$$= \sum_m \sum_{\alpha'} (\mathbf{R}^n, \alpha | \underline{W} | \mathbf{R}^m, \alpha') (\mathbf{R}^m, \alpha' | \underline{P}(t) | \mathbf{0}, \beta). \quad (2.15)$$

Now, we note that what enters into the line-shape calculation in Eq. (2.1) is the spatial Fourier transform of $(\mathbf{R}^n, \alpha | \underline{P}(t) | \mathbf{0}, \beta)$:

$$\sum_n \exp(i\mathbf{k} \cdot \mathbf{R}^n) (\mathbf{R}^n, \alpha | \underline{P}(t) | \mathbf{0}, \beta) \equiv (\alpha | \underline{P}_\mathbf{k}(t) | \beta). \quad (2.16)$$

From Eq. (2.15),

$$\frac{\partial}{\partial t} (\alpha | \underline{P}_\mathbf{k}(t) | \beta) = \sum_{\alpha'} (\alpha | \underline{W}_\mathbf{k} | \alpha') (\alpha' | \underline{P}_\mathbf{k}(t) | \beta). \quad (2.17)$$

Or, in matrix notation,

$$\frac{\partial}{\partial t} \underline{P}_\mathbf{k}(t) = \underline{W}_\mathbf{k} \underline{P}_\mathbf{k}(t). \quad (2.18)$$

In Eq. (2.18), $\underline{P}_\mathbf{k}$ and $\underline{W}_\mathbf{k}$ are matrices within the linear vector space of vacancy states only, as the dependence on the MA position has been summed over. Note also from Eq. (2.16) that

$$(\alpha | \underline{P}_\mathbf{k}(t=0) | \beta) = \sum_n \exp(i\mathbf{k} \cdot \mathbf{R}^n) \delta_{n0} \delta_{\alpha\beta} = \delta_{\alpha\beta}.$$

and hence

$$\underline{P}_\mathbf{k}(t=0) = \underline{1}. \quad (2.19)$$

Equation (2.18) in conjunction with the initial condition

neighbor shell of the MA it cannot escape. In addition, $w_1=0$ implies that the MA-vacancy pair forms a "mixed dumbbell" and the only allowed motion is the one in which the dumbbell partners exchange their position at a rate w_2 .

We have now [cf. Eq. (2.10)]

$$p_A = \frac{1}{6}, \quad p_N = 0.$$

Equation (2.26) then yields

$$\sigma_e(\mathbf{k}, \omega) = \frac{f}{\pi\hbar} \text{Re} \langle G^0 \rangle, \quad (2.33)$$

where from Eq. (2.28),

$$\langle G^0 \rangle = \frac{s + w_2 + \frac{1}{3}w_2 \sum_{i=1}^3 \cos(\mathbf{k} \cdot \mathbf{r}_i)}{s(s + 2w_2)}.$$

The line shape in Eq. (2.33) may then be written in the suggestive form

$$\begin{aligned} \sigma_e(\mathbf{k}, \omega) = & \frac{f}{2\pi\hbar} \frac{\Gamma_0/2\hbar}{(\omega - \omega_0)^2 + (\Gamma_0/2\hbar)^2} \\ & \times \left[1 + \frac{1}{3} \sum_{i=1}^3 \cos(\mathbf{k} \cdot \mathbf{r}_i) \right] \\ & + \frac{f}{2\pi\hbar} \frac{(2w_2 + \Gamma_0/2\hbar)}{(\omega - \omega_0)^2 + (2w_2 + \Gamma_0/2\hbar)^2} \\ & \times \left[1 - \frac{1}{3} \sum_{i=1}^3 \cos(\mathbf{k} \cdot \mathbf{r}_i) \right]. \end{aligned} \quad (2.34)$$

The first term represents an unbroadened "elastic" component whereas the second term represents a "quasielastic" component broadened by an amount $(2w_2 + \Gamma_0/2\hbar)$. The expressions inside the large parentheses give the respective intensities. The presence of a quasielastic line riding on top of the elastic line is a general feature of "cage" diffusion.¹³

3. $w_3=0, w_1 \gg w_2$: "uncorrelated" diffusion

The condition $w_3=0$ and hence $v=0$, implies again that the vacancy is trapped by the MA. This means that the MA always has a vacancy to jump into. In addition, the restriction $w_1 \gg w_2$ leads to a situation in which the vacancy is uniformly distributed between the nearest-neighbor sites of the MA. The MA can then jump into any of the nearest-neighbor sites without any correlation to its previous jump. The situation then resembles that of uncorrelated jumps in an empty lattice.

We have again [cf. Eq. (2.10)]

$$p_A = \frac{1}{6}, \quad p_N = 0,$$

which from Eq. (2.28) yields

$$\langle G^0 \rangle = \frac{1}{3} \sum_{i=1}^3 \frac{s + 4w_1 + w_2[1 + \cos(\mathbf{k} \cdot \mathbf{r}_i)]}{D_i}. \quad (2.35)$$

In addition, Eq. (2.27) implies

$$\bar{G}^0 = 6 \langle G^0 \rangle + \frac{1}{s - \gamma}. \quad (2.36)$$

Using the fact that $v=p_N=0$ and Eq. (2.36), we obtain from Eq. (2.26),

$$\sigma_e(\mathbf{k}, \omega) = \frac{f}{\pi\hbar} \text{Re} \left\{ \left[1 - \frac{w_1}{s - \gamma} - w_1 \left[6 \langle G^0 \rangle + \frac{1}{s - \gamma} \right]^{-1} \right] \langle G^0 \rangle \right\},$$

which simplifies to

$$\sigma_e(\mathbf{k}, \omega) = \frac{f}{\pi\hbar} \text{Re} [(\langle G^0 \rangle^{-1} - 6w_1)^{-1}]. \quad (2.37)$$

We study now the $w_1 \gg w_2$ limit. For this it is convenient first to decompose $\langle G^0 \rangle$ in Eq. (2.35) as a sum of two terms. Thus

$$\langle G^0 \rangle = \frac{1}{3} \sum_{i=1}^3 \left[\frac{C_i^-}{s + A_i^-} + \frac{C_i^+}{s + A_i^+} \right], \quad (2.38)$$

where

$$\begin{aligned} A_i^\pm &= (w_2 + 5w_1) \pm [w_1^2 + w_2^2 - 2w_1w_2 \cos(\mathbf{k} \cdot \mathbf{r}_i)]^{1/2}, \\ C_i^\pm &= \frac{1}{2} \left[1 \pm \frac{w_1 + w_2 \cos(\mathbf{k} \cdot \mathbf{r}_i)}{[w_1^2 + w_2^2 - 2w_1w_2 \cos(\mathbf{k} \cdot \mathbf{r}_i)]^{1/2}} \right]. \end{aligned} \quad (2.39)$$

When $w_1 \gg w_2$, it is easy to see that

$$\begin{aligned} A_i^+ &\simeq 6w_1 + w_2[1 - \cos(\mathbf{k} \cdot \mathbf{r}_i)], \\ A_i^- &\simeq 4w_1 + w_2[1 + \cos(\mathbf{k} \cdot \mathbf{r}_i)], \\ C_i^+ &\simeq 1, \\ C_i^- &\simeq 0. \end{aligned} \quad (2.40)$$

Equation (2.38) then yields

$$\langle G^0 \rangle \simeq \frac{1}{3} \sum_{i=1}^3 \{s + 6w_1 + w_2[1 - \cos(\mathbf{k} \cdot \mathbf{r}_i)]\}^{-1},$$

which may be written approximately as

$$\langle G^0 \rangle \simeq \frac{1}{s + 6w_1} \left[1 - \frac{1}{3} \frac{w_2}{s + 6w_1} \sum_{i=1}^3 [1 - \cos(\mathbf{k} \cdot \mathbf{r}_i)] \right].$$

Therefore,

$$\langle G^0 \rangle^{-1} \simeq (s + 6w_1) \left[1 + \frac{1}{3} \frac{w_2}{s + 6w_1} \sum_{i=1}^3 [1 - \cos(\mathbf{k} \cdot \mathbf{r}_i)] \right].$$

Equation (2.37) then leads to

$$\sigma_e(\mathbf{k}, \omega) = \frac{f}{\pi\hbar} \text{Re} \left[s + \frac{1}{3} w_2 \sum_{i=1}^3 [1 - \cos(\mathbf{k} \cdot \mathbf{r}_i)] \right]^{-1}.$$

Equation (2.41) is the Chudley-Elliott result for the sc structure.⁴

The analytical expression in Eq. (2.26) lends physical insight into the mathematical structure of the line-shape formula when we study various limits, as we have shown

above. However, in dealing with other kinds of crystal structure, it is impractical to attempt an analytic calculation as the matrix of $(s\mathbb{1} - \underline{W}_{\mathbf{k}})$ is of larger dimension. Thus, for instance, we have to deal with 9×9 and 13×13 dimensional matrices in the bcc and fcc crystals, respectively. In such cases it is more convenient to carry out the inversion of the matrix $(s\mathbb{1} - \underline{W}_{\mathbf{k}})$ numerically. The results of such computation will be discussed later in Sec. IV.

III. COMBINED EFFECTS OF DIFFUSION AND HYPERFINE INTERACTION

A. Mathematical formulation

In this section we consider the influence of hyperfine interaction on the Mössbauer line shape when the vacancy is a nearest neighbor to the MA. As mentioned in Sec. I, the hyperfine interaction manifests itself mainly in the form of isomer shift and quadrupole splitting, and it is these two effects that we shall treat in the sequel. The hyperfine interaction may then be represented by the Hamiltonian

$$\sigma_e(\mathbf{k}, \omega) = \frac{2}{2I_e + 1} \frac{f}{\pi \hbar} \text{Re} \int_0^\infty dt \exp(-st) \sum_{M_e, M_g, M'_e, M'_g} \langle I_e M_e | \mathcal{A}(\hat{\mathbf{k}}) | I_g M_g \rangle \langle I_g M'_g | \mathcal{A}^\dagger(\hat{\mathbf{k}}) | I_e M'_e \rangle \times (I_g M_g, I_e M_e | (U(t))_{\text{av}} | I_g M'_g, I_e M'_e), \quad (3.2)$$

where s is defined in Eq. (2.23), and e and g stand for the excited and ground states of the nucleus. Here $\mathcal{A}(\mathbf{k})$ represents the interaction between the nucleus and the radiation field and $\mathcal{A}^\dagger(\mathbf{k})$ its Hermitian adjoint; both depend on the direction $\hat{\mathbf{k}}$ of emission of the γ ray with respect to an arbitrarily chosen quantization axis for the nuclear spin. The entity $U(t)$ is the time-development operator associated with the Hamiltonian in Eq. (3.1), and is defined by

$$U(t) = \exp \left[\frac{i}{\hbar} \int_0^t \mathcal{H}^\alpha(t') dt' \right], \quad (3.3)$$

where $\mathcal{H}^\alpha(t)$ is the Liouville operator¹² corresponding to

$$\sigma_e(\mathbf{k}, \omega) = \frac{2}{2I_e + 1} \frac{f}{\pi \hbar} \text{Re} \sum_{M_e, M_g, M'_e, M'_g} \langle I_e M_e | \mathcal{A}(\hat{\mathbf{k}}) | I_g M_g \rangle \langle I_g M'_g | \mathcal{A}^\dagger(\hat{\mathbf{k}}) | I_e M'_e \rangle \times \sum_{\alpha, \beta} (\alpha | (I_g M_g, I_e M_e | \left[s\mathbb{1} - \frac{i}{\hbar} \sum_j V_j^\alpha \underline{F}_j - \underline{W}_{\mathbf{k}} \right]^{-1} | I_g M'_g, I_e M'_e) | \beta) p_\beta. \quad (3.4)$$

Here the matrix $\underline{W}_{\mathbf{k}}$ is defined in Eq. (2.24). The matrix \underline{F}_j projects out the j th (associated) state amongst the possible states occupied by the vacancy, i.e.,¹²

$$\begin{aligned} (\alpha | \underline{F}_j | \beta) &= \delta_{\alpha\beta} \delta_{\alpha j}, \\ V_j &= 0, \text{ if } j = N. \end{aligned} \quad (3.5)$$

$$\mathcal{H}(t) = (\Delta(I) + Q \{ 3[\mathbf{I} \cdot \hat{\mathbf{R}}_{\text{MA-v}}(t)]^2 - I^2 \}) \times \delta(R_{\text{MA-v}}(t) - d_{\text{NN}}), \quad (3.1)$$

where $R_{\text{MA-v}}(t)$ denotes the distance between the MA and the vacancy, and the δ function ensures that the hyperfine interaction becomes operative only when the vacancy is at a nearest-neighbor site, separated from the MA by a distance d_{NN} . The first term $\Delta(I)$ in Eq. (3.1) accounts for the monopole interaction between the Mössbauer nucleus and its electronic shell, which depends on the spin angular momentum state I of the nucleus. The second term represents the electric quadrupole interaction which depends on the nuclear quadrupole moment Q , and the relative orientation between \mathbf{I} and $\hat{\mathbf{R}}_{\text{MA-v}}(t)$, the unit vector joining the MA and the vacancy. In view of the fact that $\mathbf{R}_{\text{MA-v}}(t)$ is a stochastic process governed by an underlying probability which obeys Eq. (2.3), the Hamiltonian $\mathcal{H}(t)$ is also a stochastic process. The Mössbauer line shape under the influence of the Hamiltonian in Eq. (3.1) is given by¹²

$\mathcal{H}(t)$. The exponentiated operator in Eq. (3.3) should of course be suitably time ordered.

The crucial point to note here is that $(\dots)_{\text{av}}$ in $U(t)$ designates an average over the underlying stochastic process which, in the present case, concerns the kinetics of the MA-vacancy pair. The indicated averaging, therefore, has to be carried out over a stationary Markov process defined by a conditional probability which obeys the master equation (2.3). Needless to say, the outcome of the averaging procedure must then include the pure diffusion effects analyzed in Sec. II. Following the procedure of Blume¹² and taking special note of the fact that in the present application one has to perform an additional spatial Fourier transform with regard to the position of the MA (cf. Sec. II A), we obtain

Equation (3.5) is a statement of the fact that the hyperfine interaction occurs only when the vacancy is on one of the associated states. The operator V_j ($j \neq N$) represents the hyperfine Hamiltonian when the vacancy is at the j th associated state. It can be read out from Eq. (3.1). Thus, for instance, if the vacancy is on the associated state 1 or

−1 (see Fig. 3), we have

$$V_{\pm 1} = \Delta(I) + Q(3I_x^2 - I^2). \quad (3.6)$$

Similarly,

$$V_{\pm 2} = \Delta(I) + Q(3I_y^2 - I^2), \quad (3.7)$$

and

$$V_{\pm 3} = \Delta(I) + Q(3I_z^2 - I^2). \quad (3.8)$$

Note that if the hyperfine interaction vanishes ($V_j=0$), Eq. (3.4) reduces to the earlier line shape formula in Eq. (2.22).

B. Analytical results for the sc case and for ^{57}Fe

For the sake of definiteness we restrict the subsequent discussion to the ^{57}Fe isotope as the MA. The effect of a (static) hyperfine interaction on the ^{57}Fe nucleus is shown schematically in Fig. 4. The simplifying feature to note is that the quadrupole interaction vanishes in the ground state of the nucleus since $I_g = \frac{1}{2}$. This allows us to carry out further mathematical operations in terms of an ordi-

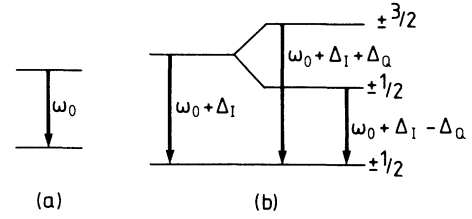


FIG. 4. Nuclear transitions for ^{57}Fe ($I_e = \frac{3}{2}$, $I_g = \frac{1}{2}$). (a) For the isolated MA the transition energy is $\hbar\omega_0$. (b) Hyperfine interactions due to NN vacancy change the nuclear transitions. The energy is shifted by the vacancy induced isomer shift; the degeneracy of the nuclear levels for $I_e = \frac{3}{2}$ is partially lifted by the quadrupole interaction due to the vacancy induced electric field gradient, the transitions of ^{57}Fe are split into a doublet.

nary operator (and not a Liouville operator), as shown below.

Writing out explicitly the matrix elements of the Liouville operator in Eq. (3.3), the basic line-shape expression in Eq. (3.2) may be rewritten as¹²

$$\begin{aligned} \sigma_e(\mathbf{k}, \omega) = & \frac{f}{2\pi\hbar} \text{Re} \int_0^\infty dt \exp(-st) \sum_{M_e, M_g, M'_e, M'_g} \langle I_e M_e | \mathcal{A}(\hat{\mathbf{k}}) | I_g M_g \rangle \langle I_g M'_g | \mathcal{A}^\dagger(\hat{\mathbf{k}}) | I_e M'_e \rangle \\ & \times \left\langle I_g M_g \left| \exp \left[\frac{i}{\hbar} \int_0^t \mathcal{H}(t') dt' \right] \right| I_g M'_g \right\rangle \\ & \times \left\langle I_e M'_e \left| \exp \left[-\frac{i}{\hbar} \int_0^t \mathcal{H}(t') dt' \right] \right| I_e M_e \right\rangle_{\text{av}}. \end{aligned} \quad (3.9)$$

Now we use the form of the Hamiltonian given in Eq. (3.1) and the fact that the quadrupole interaction is zero in the ground state. Then

$$(\dots)_{\text{av}} = \delta_{M_g M'_g} \left\langle \exp \left[\frac{i}{\hbar} \int_0^t \Delta_g(t') dt' \right] \langle I_e M'_e | \exp \left[-\frac{i}{\hbar} \int_0^t [\Delta_e(t') + V(t')] dt' \right] | I_e M_e \rangle \right\rangle_{\text{av}},$$

where $\Delta_g(t)$ represents the fluctuating monopole interaction in the ground state and $\Delta_e(t)$ the corresponding quantity in the excited state, and $V(t)$ the fluctuating quadrupolar part of the Hamiltonian. Noting that $\Delta_g(t)$ and $\Delta_e(t)$ are C number variables we may regroup them and write

$$(\dots)_{\text{av}} = \delta_{M_g M'_g} \langle I_e M'_e | \left[\exp \left[-\frac{i}{\hbar} \int_0^t [\Delta_I(t') + V(t')] dt' \right] \right]_{\text{av}} | I_e M_e \rangle,$$

where $\Delta_I(t) = \Delta_e(t) - \Delta_g(t)$ is the fluctuating isomer shift. The subsequent mathematical development is identical to that described in Sec. III A, and we have for the line shape [cf. Eq. (3.4)]

$$\begin{aligned} \sigma_e(\mathbf{k}, \omega) = & \frac{f}{2\pi\hbar} \text{Re} \sum_{M_e, M_g, M'_e} \langle I_e M_e | \mathcal{A}(\hat{\mathbf{k}}) | I_g M_g \rangle \langle I_g M'_g | \mathcal{A}^\dagger(\hat{\mathbf{k}}) | I_e M'_e \rangle \\ & \times \sum_{\alpha, \beta} (\alpha | \langle M'_e | \left[s \mathbb{1} - \frac{i}{\hbar} \sum_j V_j \mathbf{F}_j - \mathbf{W} \cdot \mathbf{k} \right]^{-1} | M_e \rangle | \beta) p_\beta. \end{aligned} \quad (3.10)$$

In Eq. (3.10), V_j is an ordinary operator which is given, for example, in the sc case by Eqs. (3.6)–(3.8), with $\Delta(I)$ now interpreted as the isomer shift. Equation (3.10) can be expressed in a somewhat more compact shape as

$$\sigma_e(\mathbf{k}, \omega) = \frac{f}{2\pi\hbar} \operatorname{Re} \sum_{M_e, M'_e} \mathcal{D}_{M_e M'_e}(\hat{\mathbf{k}}) \langle M'_e | (\tilde{U}(s, \mathbf{k}))_{\text{av}} | M_e \rangle, \quad (3.11)$$

where

$$\mathcal{D}_{M_e M'_e}(\hat{\mathbf{k}}) = \sum_{M_g} \langle I_e M_e | \mathcal{A}(\hat{\mathbf{k}}) | I_g M_g \rangle \times \langle I_g M_g | \mathcal{A}^\dagger(\hat{\mathbf{k}}) | I_e M'_e \rangle, \quad (3.12)$$

$$\tilde{U}(s, \mathbf{k}) = \left[s \mathbb{1} - \frac{i}{\hbar} \sum_j V_j F_j - \underline{W}_{\mathbf{k}} \right]^{-1}, \quad (3.13)$$

and

$$(\tilde{U}(s, \mathbf{k}))_{\text{av}} = \sum_{\alpha, \beta} (\alpha | \tilde{U}(s, \mathbf{k}) | \beta) p_\beta. \quad (3.14)$$

In the case of ^{57}Fe for which $I_e = \frac{3}{2}$ and $I_g = \frac{1}{2}$, the matrix of \mathcal{D} (of dimension 4×4) has 12 nonvanishing elements which are given as¹⁴

$$\begin{aligned} \langle \frac{1}{2} | (\tilde{U}(s, \mathbf{k}))_{\text{av}} | \frac{1}{2} \rangle &= \langle -\frac{1}{2} | (\tilde{U}(s, \mathbf{k}))_{\text{av}} | -\frac{1}{2} \rangle \\ &= (H_1 H_3 - H_2^2)^{-1} [H_1(H_4 + H_5 - H_6 - H_7 + H_8) + \sqrt{3}H_2(H_6 - H_7)], \\ \langle \frac{3}{2} | (\tilde{U}(s, \mathbf{k}))_{\text{av}} | \frac{3}{2} \rangle &= \langle -\frac{3}{2} | (\tilde{U}(s, \mathbf{k}))_{\text{av}} | -\frac{3}{2} \rangle \\ &= (H_1 H_3 - H_2^2)^{-1} [H_3(H_4 + H_5 + H_6 + H_7 - H_8) + \sqrt{3}H_2(H_6 - H_7)], \\ \langle \frac{3}{2} | (\tilde{U}(s, \mathbf{k}))_{\text{av}} | -\frac{1}{2} \rangle &= \langle -\frac{3}{2} | (\tilde{U}(s, \mathbf{k}))_{\text{av}} | \frac{1}{2} \rangle \\ &= -(H_1 H_3 - H_2^2)^{-1} [H_2(H_4 + H_5 - H_6 - H_7 + H_8) + \sqrt{3}H_3(H_6 - H_7)], \\ \langle \frac{1}{2} | (\tilde{U}(s, \mathbf{k}))_{\text{av}} | -\frac{3}{2} \rangle &= \langle -\frac{1}{2} | (\tilde{U}(s, \mathbf{k}))_{\text{av}} | \frac{3}{2} \rangle \\ &= -(H_1 H_3 - H_2^2)^{-1} [H_2(H_4 + H_5 + H_6 + H_7 - H_8) + \sqrt{3}H_1(H_6 - H_7)], \end{aligned} \quad (3.16)$$

where

$$\begin{aligned} H_1 &= \tilde{A}_0 - \frac{i}{\hbar} Q \left(\frac{1}{2} \tilde{B}_1 + \frac{1}{2} \tilde{B}_2 - \tilde{B}_3 \right), \\ H_2 &= \frac{\sqrt{3}}{2} \frac{i}{\hbar} Q (\tilde{B}_1 - \tilde{B}_2), \\ H_3 &= \tilde{A}_0 + \frac{i}{\hbar} Q \left(\frac{1}{2} \tilde{B}_1 + \frac{1}{2} \tilde{B}_2 - \tilde{B}_3 \right), \\ H_4 &= \frac{1}{s - \gamma} (p_N - p_A), \end{aligned} \quad (3.17)$$

$$\begin{aligned} \langle \frac{3}{2} | \mathcal{D} | \frac{3}{2} \rangle &= \langle -\frac{3}{2} | \mathcal{D} | -\frac{3}{2} \rangle = \frac{1}{2} + \frac{1}{8} (3 \cos^2 \theta - 1), \\ \langle \frac{1}{2} | \mathcal{D} | \frac{1}{2} \rangle &= \langle -\frac{1}{2} | \mathcal{D} | -\frac{1}{2} \rangle = \frac{1}{2} - \frac{1}{8} (3 \cos^2 \theta - 1), \\ \langle -\frac{1}{2} | \mathcal{D} | -\frac{3}{2} \rangle &= -\langle \frac{3}{2} | \mathcal{D} | \frac{1}{2} \rangle = \frac{\sqrt{3}}{8} \sin(2\theta) \exp(-i\phi), \end{aligned} \quad (3.15)$$

$$\langle -\frac{3}{2} | \mathcal{D} | -\frac{1}{2} \rangle = -\langle \frac{1}{2} | \mathcal{D} | \frac{3}{2} \rangle = \frac{\sqrt{3}}{8} \sin(2\theta) \exp(i\phi),$$

$$\langle \frac{3}{2} | \mathcal{D} | -\frac{1}{2} \rangle = \langle \frac{1}{2} | \mathcal{D} | -\frac{3}{2} \rangle = \frac{\sqrt{3}}{8} \sin^2 \theta \exp(-2i\phi),$$

$$\langle -\frac{1}{2} | \mathcal{D} | \frac{3}{2} \rangle = \langle -\frac{3}{2} | \mathcal{D} | \frac{1}{2} \rangle = \frac{\sqrt{3}}{8} \sin^2 \theta \exp(2i\phi),$$

θ and ϕ being the directions of $\hat{\mathbf{k}}$ with respect to the quantization axis for the nuclear spin, chosen to lie along the z direction.

Our main task now is to evaluate the matrix elements of $(\tilde{U}(s, \mathbf{k}))_{\text{av}}$ which is also a 4×4 matrix within the nuclear angular momentum space. In order to do this it is clear from Eq. (3.13) that we have to invert a 28×28 matrix. This is because the matrix of $\tilde{U}(s, \mathbf{k})$ is labeled by four angular momentum indices and seven stochastic indices, in the sc case. Again for the sc case, we show in Appendix B how the required mathematical operations can be carried out completely analytically. From the results given in Appendix B it turns out that $(\tilde{U}(s, \mathbf{k}))_{\text{av}}$ has only eight (out of sixteen) nonvanishing elements which are enumerated below:

$$H_5 = A_0 \left[p_A + p_N \frac{\lambda - w_1}{s + \nu + 6\lambda} \right],$$

$$H_6 = \frac{1}{2} \frac{i}{\hbar} Q B_1 \left[p_A + p_N \frac{\lambda - w_1}{s + \nu + 6\lambda} \right],$$

$$H_7 = \frac{1}{2} \frac{i}{\hbar} Q B_2 \left[p_A + p_N \frac{\lambda - w_1}{s + \nu + 6\lambda} \right],$$

$$H_8 = \frac{1}{2} \frac{i}{\hbar} Q B_3 \left[p_A + p_N \frac{\lambda - w_1}{s + \nu + 6\lambda} \right],$$

$$A_0 = 2 \sum_{i=1}^3 \left[\frac{C_i^+ q_i^+}{(q_i^+)^2 + \frac{Q^2}{\hbar^2}} + \frac{C_i^- q_i^-}{(q_i^-)^2 + \frac{Q^2}{\hbar^2}} \right] + \frac{1}{s - \gamma},$$

$$\tilde{A}_0 = 1 - \frac{\nu - w_1}{s - \gamma} - A_0 \frac{w_1(s - \gamma) + (\nu - w_1)(\lambda - w_1)}{s + \nu + 6\lambda},$$

$$B_i = 2 \left[\frac{C_i^+}{(q_i^+)^2 + \frac{Q^2}{\hbar^2}} + \frac{C_i^-}{(q_i^-)^2 + \frac{Q^2}{\hbar^2}} \right], \quad i = 1, 2, 3,$$

$$\tilde{B}_i = B_i \frac{w_1(s - \gamma) + (\nu - w_1)(\lambda - w_1)}{(s + \nu + 6\lambda)}, \quad i = 1, 2, 3,$$

$$q_i^\pm = s + \nu + \frac{i}{\hbar} \Delta(I) + A_i^\pm, \quad i = 1, 2, 3,$$

(3.18)

and A_i^\pm and C_i^\pm have already been defined in Eq. (2.39).

Before we present the lineshape plots based on the above formulas, it is useful to consider certain limiting cases.

1. $\Delta(I) = 0, Q = 0$: vanishing hyperfine interaction

In this case,

$$H_1 = H_3 = \tilde{A}_0, \quad H_2 = H_4 = H_5 = H_6 = H_7 = H_8 = 0, \quad (3.19)$$

where now,

$$A_0 = 2 \sum_{i=1}^3 \left[\frac{C_i^+}{s + \nu + A_i^+} + \frac{C_i^-}{s + \nu + A_i^-} \right] + \frac{1}{s - \gamma}. \quad (3.20)$$

From Eq. (3.16) then follows that all the off-diagonal elements of $(\tilde{U}(s, \mathbf{k}))_{av}$ are zero, and all the diagonal elements are equal. Thus

$$\langle M_e' | (\tilde{U}(s, \mathbf{k}))_{av} | M_e \rangle = \delta_{M_e M_e'} \frac{(H_4 + H_5)}{H_1}, \quad (3.21)$$

independent of M_e .

Substituting Eq. (3.21) in Eq. (3.11), we have

$$\sigma_e(\mathbf{k}, \omega) = \frac{f}{2\pi\hbar} \operatorname{Re} \left[\frac{(H_4 + H_5)}{H_1} \sum_{M_e} \mathcal{D}_{M_e M_e}(\hat{\mathbf{k}}) \right]$$

$$= \frac{f}{\pi\hbar} \operatorname{Re} \left[\frac{(H_4 + H_5)}{H_1} \right], \quad (3.22)$$

where the last step follows from Eq. (3.15).

Now, it may be easily checked that A_0 given in Eq. (3.20) is identical with \bar{G}^0 defined earlier in Eq. (3.27). From Eqs. (3.18) and (3.19) then follows that

$$H_1 = 1 - \frac{\nu - w_1}{s - \gamma} - \frac{w_1(s - \gamma) + (\nu - w_1)(\lambda - w_1)}{s + \nu + 6\lambda} \bar{G}^0. \quad (3.23)$$

Next, from Eqs. (3.17) and (3.20),

$$H_4 + H_5 = \frac{p_N}{s - \gamma} + 2p_A \sum_{i=1}^3 \left[\frac{C_i^+}{s + \nu + A_i^+} + \frac{C_i^-}{s + \nu + A_i^-} \right]$$

$$+ p_N \frac{\lambda - w_1}{s + \nu + 6\lambda} \bar{G}^0$$

$$= \langle G^0 \rangle + p_N \frac{\lambda - w_1}{s + \nu + 6\lambda} \bar{G}^0, \quad (3.24)$$

where $\langle G^0 \rangle$ is given earlier in Eq. (2.28). Equation (3.22), together with Eqs. (3.23) and (3.24), lead to a line-shape expression which is identical with Eq. (2.26) derived before, therefore, as expected, when the hyperfine interactions vanish, the formula (3.11) yields the line shape for the pure diffusion case.

2. $w_2 = 0$: Pure "relaxation" effects

In this case we "switch off" the MA-vacancy exchange, as in Sec. II B 1. The only effect the vacancy motion has on the MA is to induce "relaxation" via fluctuations in the hyperfine interaction. This happens due to two reasons: (i) when the vacancy jumps from a nearest-neighbor site to a non-nearest-neighbor site (i.e., a non-associated state) both the isomer shift and the quadrupolar interaction vanish; (ii) when the vacancy jumps within the nearest-neighbor shell of the MA (i.e., the associated states) the quadrupolar interaction changes form although the isomer shift stays constant. Thus the line shape now should be identical with that due to interstitial diffusion in the vicinity of the MA, a mechanism that is important in other systems.¹⁵

Setting $w_2 = 0$ we obtain from Eq. (2.39)

$$A_i^+ = 6w_1, \quad A_i^- = 4w_1, \quad C_i^+ = 1, \quad C_i^- = 0,$$

which from Eq. (3.18) imply that

$$B_1 = B_2 = B_3; \quad \tilde{B}_1 = \tilde{B}_2 = \tilde{B}_3.$$

Hence from Eq. (3.17),

$$H_2 = 0, \quad H_1 = H_3 = \tilde{A}_0, \quad (3.25)$$

$$H_6 = H_7 = \frac{1}{2} H_8 = \frac{1}{2} \frac{i}{\hbar} Q B_1 \left[p_A + p_N \frac{\lambda - w_1}{s + \nu + 6\lambda} \right].$$

Again we find from Eq. (3.16) that all the off-diagonal elements of $(\tilde{U}(s, \mathbf{k}))_{av}$ are zero and all the diagonal elements are equal; Eq. (3.21) and hence Eq. (3.22) still hold good but now [cf. Eq. (3.18)]

$$A_0 = 6 \frac{s + \nu + 6w_1 + \frac{i}{\hbar} \Delta(I)}{\left[s + \nu + 6w_1 + \frac{i}{\hbar} \Delta(I) \right]^2 + Q^2/\hbar^2} + \frac{1}{s - \gamma}. \quad (3.26)$$

Using then Eq. (3.22) the line shape is given by

$$\sigma_e(\mathbf{k}, \omega) = \frac{f}{\pi\hbar} \operatorname{Re} \left\{ \left[1 - \frac{\nu - w_1}{s - \gamma} - A_0 \frac{w_1(s - \gamma) + (\nu - w_1)(\lambda - w_1)}{s + \nu + 6\lambda} \right]^{-1} \left[\frac{p_N - p_A}{s - \gamma} + A_0 \left[p_A + p_N \frac{\lambda - w_1}{s + \nu + 6\lambda} \right] \right] \right\}, \quad (3.27)$$

where A_0 is to be obtained from Eq. (3.26). Apart from a rescaling of the rate parameters (necessitated by a change to the bcc system) the result (3.27) is identical to the line-shape formula derived earlier in the context of interstitial motion (e.g., of carbon) in bcc iron.¹⁵

3. $w_2=0$ and $w_3=0$: Pure quadrupolar relaxations

Here we ignore the exchange motion as in Sec. II B 2 above; in addition, we restrict the motion of the vacancy to the nearest-neighbor shell of the MA (i.e., the associated states). Therefore, the only effect to be considered is that due to random changes in the direction of the electric field gradient leading to quadrupolar relaxations.

The line-shape expression relevant to the present instance is again given by Eq. (3.27) in which we have to additionally set $w_2 = \nu = 0$, and $p_A = \frac{1}{6}$, $p_N = 0$ [cf. Eq. (2.10)]. Thus,

$$\begin{aligned} \sigma_e(\mathbf{k}, \omega) &= \frac{f}{\pi\hbar} \operatorname{Re} \left\{ \left[1 - w_1 \left[A_0 - \frac{1}{s - \gamma} \right] \right]^{-1} \frac{1}{6} \left[A_0 - \frac{1}{s - \gamma} \right] \right\} = \frac{f}{\pi\hbar} \operatorname{Re} \left[6 \left[A_0 - \frac{1}{s - \gamma} \right]^{-1} - 6w_1 \right]^{-1} \\ &= \frac{f}{\pi\hbar} \operatorname{Re} \left[s + \frac{i}{\hbar} \Delta(I) + \frac{Q^2/\hbar^2}{s + 6w_1 + \frac{i}{\hbar} \Delta(I)} \right]^{-1}. \end{aligned} \quad (3.28)$$

Equation (3.28) yields the result derived by Tjon and Blume in an equivalent situation.¹⁶

IV. NUMERICAL CALCULATIONS

The analytical results for the Mössbauer emission spectrum are quite complicated even for the simple cubic lattice. We therefore have performed numerical calculations for the three cubic lattices. We shall discuss the general procedure, but for the sake of brevity present results for the fcc lattice only.

The general problem is the calculation of the matrix

$$\tilde{U}(s, \mathbf{k}) = \left[s \mathbb{1} - (i/\hbar) \sum_j V_j \mathbf{E}_j - \underline{W}_k \right]^{-1} \quad (4.1)$$

as defined already in Eq. (3.13). $\tilde{U}(s, \mathbf{k})$ acts on the spin in the excited state of the Mössbauer nucleus and on the environmental states. For our stochastic jump model there are $Z + 1$ environmental states and for the case of ^{57}Fe ($I_e = \frac{3}{2}$ in the excited state) there are four spin states. Thus $\tilde{U}(s, \mathbf{k})$ is a complex $4(Z + 1)$ -dimensional square matrix. To calculate the emission spectrum $\tilde{U}(s, \mathbf{k})$ has to be evaluated for each frequency ω and emission direction k , then averaged over the environmental states according

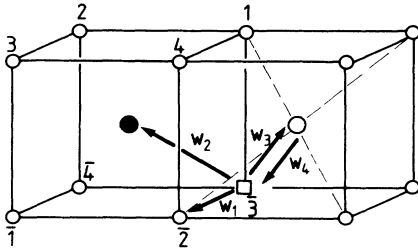


FIG. 5. Enumeration of the NN sites of the MA (●) in bcc lattices and vacancy (□) jump frequencies in the NN shell of the MA.

to Eq. (3.14) and multiplied by $\mathcal{D}_{M_e M_e'}$, given in Eq. (3.15) for $I = \frac{3}{2}$.

First, we have to set up the matrix \underline{W}_k which describes transitions between different states in the environmental space. For the sc lattice \underline{W}_k has been presented in Sec. II; for the bcc and fcc lattices we follow similar rules for the construction. The geometry of the nearest-neighbor (NN) shell is sketched in Figs. 5 and 6 for the bcc and fcc lattices, respectively. In Table I we have collected some relevant parameters of our model for the three cubic lattices. The number of sites in the NN shell of the MA is Z . The rotation of the vacancy in the NN shell proceeds via next-nearest-neighbor (NNN) jumps in sc and bcc lattices, and via NN jumps in fcc crystals. N_{w_1} is the number of sites in the NN shell which can be reached from one particular NN site by a w_1 jump, and N_{w_3} is the number of non NN sites reached by dissociation jumps with rate w_3 from a NN site. Association jumps to a NN site with rate w_4 can originate from the same number of non NN sites. Due to the different rates for dissociation and association jumps the matrix \underline{W}_k is not Hermitian. The

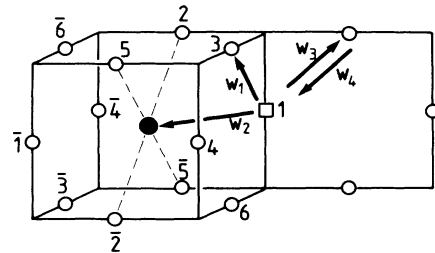


FIG. 6. Enumeration of the NN sites of the MA (●) in fcc lattices and vacancy (□) jump frequencies in the NN shell of the MA [five-frequency model of LeClaire (Ref. 9)].

TABLE I. Characteristics of jump model in cubic lattices. (For an explanation of symbols and abbreviations see text.)

Lattice	Z	Type of w_1 jump	N_{w_1}	N_{w_3}	D
sc	6	NNN	4	5	28
bcc	8	NNN	3	7	36
fcc	12	NN	4	7	52

dimension D of the matrix $\tilde{U}(s, \mathbf{k})$ is also given in Table I for the case of ^{57}Fe ($J_e = \frac{3}{2}$), i.e., $D = 4(Z + 1)$.

Second, the hyperfine interaction V_j induced by a vacancy on a NN site j ($j = 1$ to Z) is calculated according to Eq. (3.1). For $j = Z + 1$, i.e., the environmental state with no vacancy in the NN shell, the hyperfine interaction is set equal to zero.

To perform the matrix inversion of the non-Hermitian complex matrix inside the brackets in Eq. (4.1) we used the Harwell Library Routine MA23BD. The results were checked by multiplying the original matrix with the inverted one. They proved to be very reliable, the deviation of the product from the unit matrix was of the order of the computer accuracy in double precision for a single matrix element.

To generate a Mössbauer spectrum as shown, e.g., in Fig. 7, we have calculated $\tilde{U}(s, \mathbf{k})$ for typically 101 different frequencies and 41 emission directions in the $\{110\}$ plane (azimuth angle $\phi = 45^\circ$) varying the polar angle θ from 0° ([001] direction) to 90° ([110] direction).

We will now discuss the results for various choices of the vacancy jump rates and the hyperfine interaction parameters. In Table II we have collected the parameters used in the calculations.

A. Pure diffusion broadening

Figure 7 shows the Mössbauer emission spectrum for the self-diffusion case with hyperfine interaction set equal to zero. The three-dimensional plot, Fig. 7(a), shows the intensity $\sigma(\theta, \omega)$ on the z axis, the frequency $\omega - \omega_0$ (in units of the natural linewidth Γ_0) on the x axis, and the polar angle θ on the y axis. The intensity is normalized such that the integral over frequencies is equal to $\pi/2$.

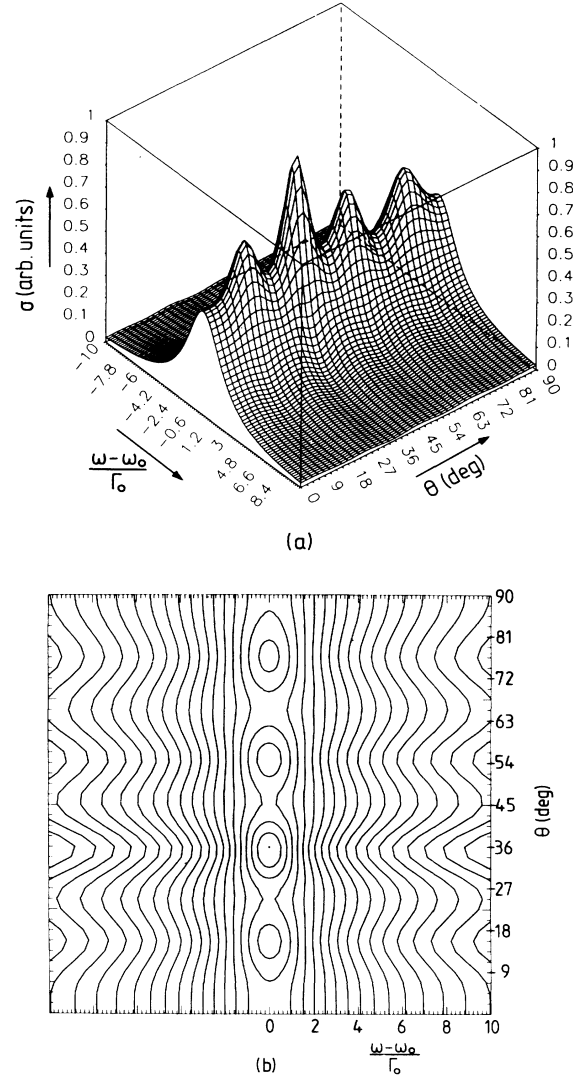


FIG. 7. Mössbauer spectrum $\sigma(\theta, \omega)$ as a function of emission frequency ω and emission angle θ in the (110) plane. The parameters are chosen to describe pure diffusion broadening for self diffusion in an fcc lattice (see text and Table II). (a) Three-dimensional plot: σ , z axis; θ , y axis; $\omega - \omega_0$, x axis. (b) Contour plot for intensity values calculated according to Eq. (4.2).

TABLE II. Parameter sets used for spectra shown in the figures. All figures are for fcc crystals with cubic lattice constant of Al, $a = 0.413$ nm, and γ ray of ^{57}Fe , $|k| = 72.97$ (nm) $^{-1}$, $\Gamma_0 = 4.67 \times 10^{-9}$ eV.

Figs.	Γ_0 HWHH (mm/sec)	Δ/Γ_0	Q/Γ_0	w_1/Γ_0	w_2/Γ_0	w_3/Γ_0	w_4/Γ_0	C_v
7,8	0.1	0	0	10^3	10^3	10^3	10^3	10^{-4}
9,10	0.1	2	0	2	2	5×10^{-3}	5×10^{-3}	0.1
11	0.1	2	0	2	2	0.1	0.1	0.1
12	0.1	2	0	2	2	2	2	0.1
13	0.1	0	2	0	10	10^{-2}	10^{-2}	0.1
14	0.1	2	2	0.5	2	5×10^{-3}	5×10^{-3}	0.1
15	0.1	2	2	130	6	0.8	30	8×10^{-4}

Figure 7(b) shows a contour plot of the intensity in the (ω, θ) plane. The contour lines shown are for intensity values calculated according to

$$\begin{aligned}\sigma_i &= (\sigma_{\min} + \epsilon)\alpha^i, \\ \alpha &= (\sigma_{\max} - \epsilon)/(\sigma_{\min} + \epsilon),\end{aligned}\quad (4.2)$$

where σ_{\min} and σ_{\max} are the minimum and maximum of the intensity for the shown spectra, and $\epsilon = 3 \times 10^{-3}$. The actual values are listed in Table III. The same arrangement is used for the graphs that follow. We shall use the Mössbauer line of ^{57}Fe and the fcc Al lattice as reference systems, i.e., we use $|\mathbf{k}| = 72.97 \text{ nm}^{-1}$ for the wave vector and $a = 0.413 \text{ nm}$ for the cubic lattice constant. The jump frequencies for Fig. 7 are chosen to be $w_i = 10^3 \Gamma_0$ ($i = 1, 4$) (Γ_0 is the natural linewidth). The average vacancy concentration is set to $c_v = 10^{-4}$. This means that the average rate of formation of a NN-vacancy-MA complex which is given by $7w_4c_v$ is of the order of the natural linewidth. This rate essentially determines the diffusion induced linewidth. As discussed before,^{1,17} the anisotropy of the additional linewidth is due to the discrete jump vectors in the underlying lattice which can induce only certain phase shifts of the emitted γ ray. Thus as a function of the wavelength and emission direction the width is a periodic function in the reciprocal lattice. Whenever the Ewald sphere of the emitted γ ray comes close to a reciprocal-lattice vector of the diffusion lattice the diffusion-induced width goes to zero and the emitted line has the natural linewidth Γ_0 . In our case this is best fulfilled for $\theta = 37^\circ$ where the intensity plot shows a high maximum at $\omega = \omega_0$.

Previously,^{1,5} this model was only treated for the case of w_1 being much larger than any other vacancy jump frequency. As discussed by Mantl *et al.*¹ the model then cannot describe correlation between successive jumps of the MA. A vacancy entering the NN shell of the MA is quickly redistributed among all NN sites before any other jump can take place. Thus the direction of a particular jump of the MA is independent of the previous jump directions. In our more general treatment correlation effects are included since we can allow for different orders of magnitude of the jump frequencies and keep track of the motion of the vacancy in the NN shell. The effect can be seen in the anisotropy of the linewidth yielded by the present calculation. We have obtained the anisotropy of the diffusion induced linewidth by computer fitting a Lorentzian line to the calculated spectrum, one for each

emission direction, and subtracting the natural linewidth.

It should be mentioned that also for small vacancy concentrations c_v the spectrum actually consists of two Lorentzian lines.¹ One line is the so-called “no-vacancy line” which for the chosen parameter values carries the overwhelming part of the intensity, namely $1 - 12c_v$. This is the line to be compared to the encounter model.^{1,7,8,17} The other line is the “associated-vacancy line”. It carries only an intensity $12c_v$, and its linewidth is directly proportional to the vacancy jump rates (without the factor c_v). This line is due to the local motion of one particular vacancy in the NN shell of the MA, and it is missed in the encounter model.¹

Figure 8 shows the results of the one line fit compared to the results for the encounter model with the same jump frequencies and vacancy concentration.¹⁷ As can be seen, the two approaches show reasonable agreement. Minor differences are due to the fact that in our present model the diffusion path of a vacancy is followed in detail only in the NN shell of the MA, whereas in the encounter model all paths are considered. On the other hand, the present treatment allows for interference of diffusional broadening with hyperfine interactions which we will now consider.

B. Diffusion and fluctuating hyperfine interaction

1. Isomer shift

With our model we can treat the influence of isomer shift for a more general choice of jump frequencies than was done in the paper by Mantl *et al.*¹ Throughout the treatment we shall set the isomer shift $\Delta = 2\Gamma_0$ in order to clearly separate the emission line of static MA's being associated with a NN vacancy from that of MA's without a vacancy. We have calculated the spectrum for the same vacancy jump frequencies and concentration as used for Fig. 7, which describes self-diffusion. The spectrum turns out to be indistinguishable from Fig. 7, which at first

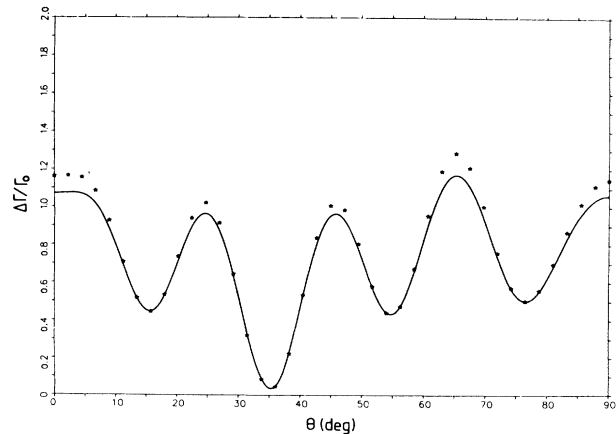


FIG. 8. Anisotropy of the diffusion induced linewidth as a function of emission angle θ (asterisks). The linewidths are obtained by fitting a single Lorentzian line to each of the spectra presented in Fig. 7. For comparison, the results of the encounter model calculation (Ref. 17) for the same parameters are shown (solid line).

TABLE III. Parameter values for contour plots.

Fig.	σ_{\min}	σ_{\max}	ϵ	α
7(b)	0.0103	0.9561	0.003	1.2521
9(b)	8.547×10^{-3}	0.6053	0.003	1.23136
11(b)	8.635×10^{-3}	0.7039	0.003	1.2407
12(b)	8.643×10^{-3}	0.9252	0.003	1.2587
13(b)	0.022	0.4433	0.003	1.16297
14(b)	0.0158	0.4972	0.003	1.18774
15(b)	9.962×10^{-3}	0.8506	0.003	1.2461

sight might be surprising. But one can notice that the weight of the isomer shifted line determined by the ratio $7w_4/c_v/w_3=7c_v$ is small ($\approx 10^{-3}$) and the fluctuation rates w_3 and $7w_4c_v$ are comparable to the magnitude of the isomer shift. As is well known in this case, the isomer shift is nearly averaged out and a single line is obtained whose width is determined by the ratio of the magnitude of the isomer shift to the fluctuation rate. For large fluctuation rates the additional width goes to zero and a line with the natural linewidth Γ_0 emerges (motional narrowing¹⁸). The average isomer shift is nearly zero because of the small weight of the isomer shifted "associated" states.

To obtain separate lines we have to lower the fluctuation rates and increase the weight of the isomer shifted line. For this purpose we have chosen $c_v=0.1$, then the weights of the isomer shifted associated states and of the nonshifted nonassociated state are almost equal. The vacancy concentration $c_v=0.1$ is probably already beyond the limit of validity of our truncated model (which neglects association of more than one vacancy in the NN shell), and we have used such a high value only for clearer representation of the effects. Figure 9 shows a spectrum with isomer shift. The jump frequencies governing the vacancy motion in the NN shell are $w_1=w_2=\Delta=2\Gamma_0$. These jumps do not contribute to the fluctuation rate of the isomer shift, i.e., to the mixing of the lines, but they determine the anisotropy of the width of the isomer shifted line since they enter decisively in the diffusion kinetics of the MA (see below). The dissociation and association rates are $w_3=w_4=0.005\Gamma_0$ and the vacancy concentration is $c_v=0.1$. With these parameters the weights of the associated and dissociated states are $12p_A = \frac{5}{11} = 0.5454$ and $p_N = \frac{5}{11} = 0.4545$, respectively. The fluctuation rates are small compared to the magnitude of the isomer shift. In Fig. 9 one can distinguish two lines, one at $\omega_1 - \omega_0 \approx 0$ and one at $\omega_2 - \omega_0 \approx \Delta = 2\Gamma_0$. Figure 10 shows the widths of two Lorentzian lines fitted to the calculated spectrum of Fig. 9. The shifted line shows a strongly anisotropic width induced by the diffusion jumps of the MA. Like in the case of pure diffusion the magnitude of the diffusion induced anisotropic width is determined by the vacancy jump frequencies in the NN shell of the MA. For our choice of parameters it is comparable to or even larger than the natural linewidth Γ_0 . The unshifted line which is due to the nonassociated MA's does not have an anisotropy of its own, the apparent anisotropy comes from the overlap with the shifted line for the vacancy-associated MA's. This can be shown analytically in the limit $c_v \ll 1$ and $w_3 \ll w_2 \ll w_1$ from the results of Ref. 1. The width of the unshifted line (nonassociated state) is then given by

$$\Gamma_N = \Gamma_0 + 84c_v w_3 \quad (4.3)$$

and the width of the shifted line (associated state) is

$$\Gamma_A = \Gamma_0 + 7w_3 + w_2 [1 - s(k)] \quad (4.4)$$

By increasing the association and dissociation rates the clearcut distinction between the two lines is lost since gradually motional averaging begins. This can be seen in

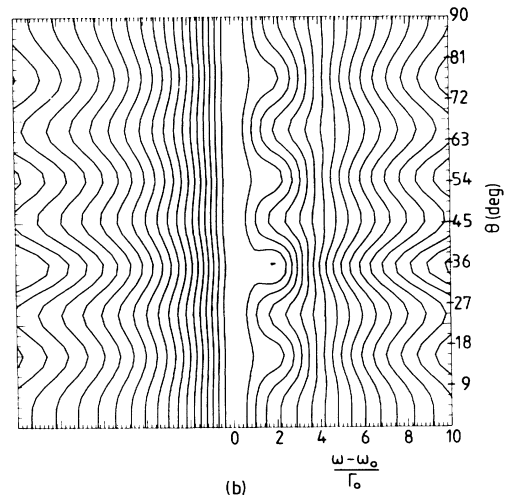
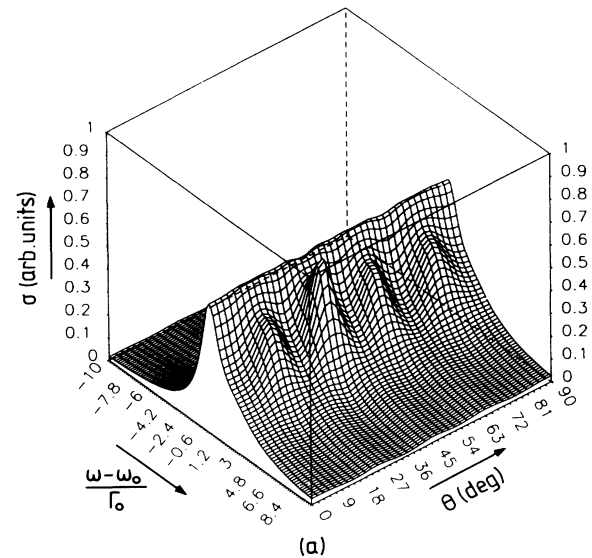


FIG. 9. Mössbauer spectra including isomer shift and diffusion broadening for the parameters listed in Table II. Arrangement of plots as in Fig. 7.

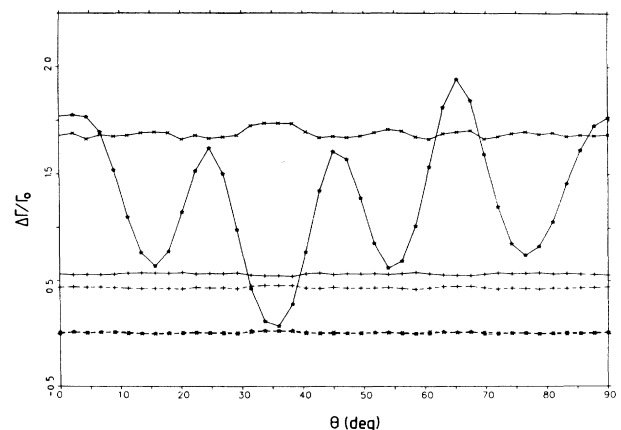


FIG. 10. Computer fit of two Lorentzian lines to each of the spectra shown as a function of emission angle in Fig. 9. Different symbols refer to different properties of the lines: \times , location; $*$, width; $+$, weight. Solid lines refer to the associated state; dotted lines to the dissociated state.

Figs. 11 and 12. For $w_3=w_4=0.1\Gamma_0$ the MA most probably changes the association state during the lifetime of the excited state. Thus the spectrum in Fig. 11 shows a dynamically averaged isomer shift. The averaging is not complete for the chosen parameters as can be seen from the remaining asymmetry of the spectrum. In this case the spectrum cannot be represented by a superposition of Lorentzian lines. For $w_3=w_4=2\Gamma_0$ the fluctuation rate of the isomer shift is so large that the spectrum in Fig. 12 shows complete averaging. It only contains symmetrical lines centered at $\langle \Delta \rangle = p_A \Delta \neq 0$, with diffusion induced anisotropic width.

2. Quadrupole interaction

We now discuss the influence of the quadrupole interaction, for the spectra shown we use $Q=2\Gamma_0$ and $\Delta=2\Gamma_0$ or $\Delta=0$. The quadrupole interaction induces a splitting of the associated line into a doublet. The spectrum con-

sists of a line centered at ω_0 resulting from the MA's not associated with a vacancy during the emission of the γ ray and an isomer shifted doublet at $\omega_1-\omega_0=\Delta-3Q$ and $\omega_2-\omega_0=\Delta+3Q$ resulting from the MA's with a vacancy in the NN shell. The doublet is anisotropically broadened due to the diffusion jumps in the MA. This can clearly be seen in Fig. 13 where we have used $\Delta=0$, $c_v=0.1$, $w_1=0$, $w_2=10\Gamma_0$, and $w_3=w_4=0.01\Gamma_0$.

As can be seen from the contour plot the anisotropy is different for the two components of the doublet, i.e., the spectrum is asymmetric although $\Delta=0$. This comes from the interference of the anisotropy induced by the quadrupole interaction (the emission line looks different along the axis of the electric field gradient and perpendicular to this axis⁵) and the phase shifts induced by the diffusion jumps. One could term this asymmetry effect the diffusion induced "dynamic" Goldanskii-Karyagin effect¹⁹ in analogy

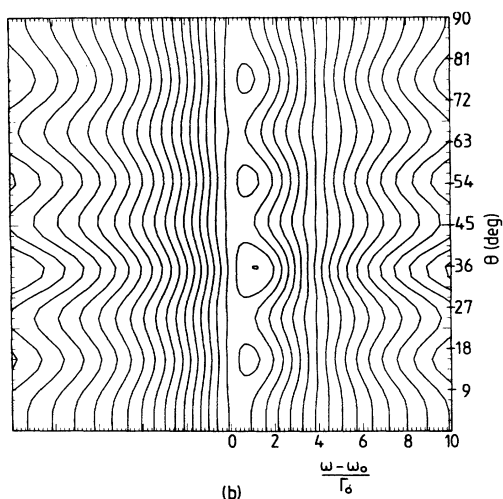
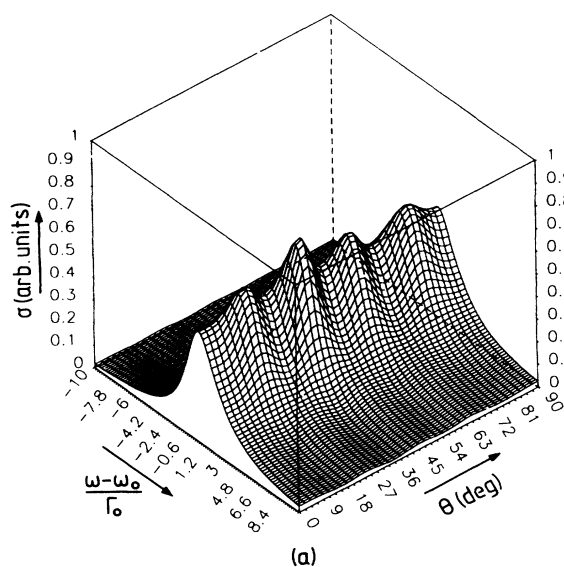


FIG. 11. Mössbauer spectra showing partial averaging of isomer shift due to larger association and dissociation rates (for parameters see Table II).

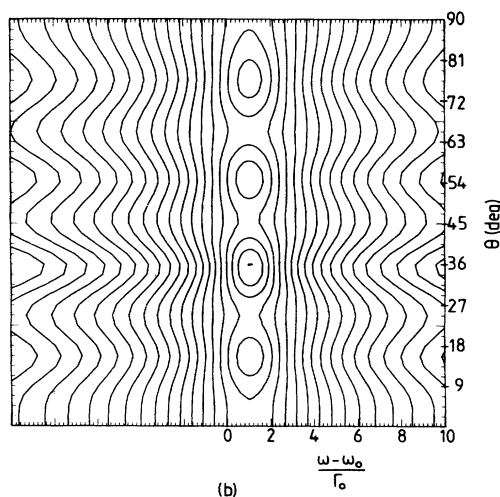
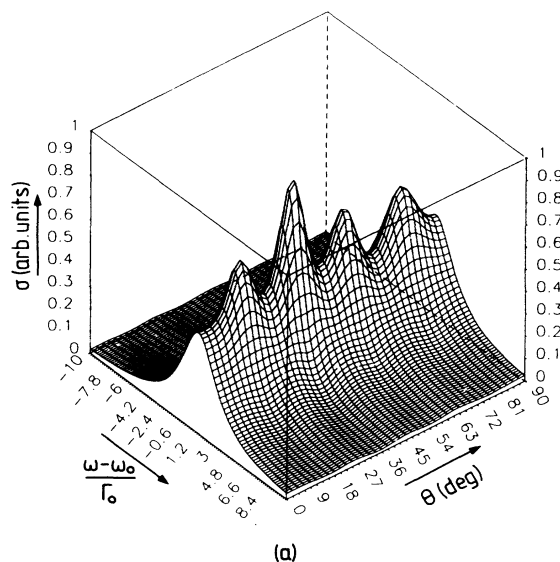


FIG. 12. Mössbauer spectra showing complete averaging of isomer shift due to very large association and dissociation rates. The lines are centered at $\langle \Delta \rangle \neq 0$ (for parameters see Table II).

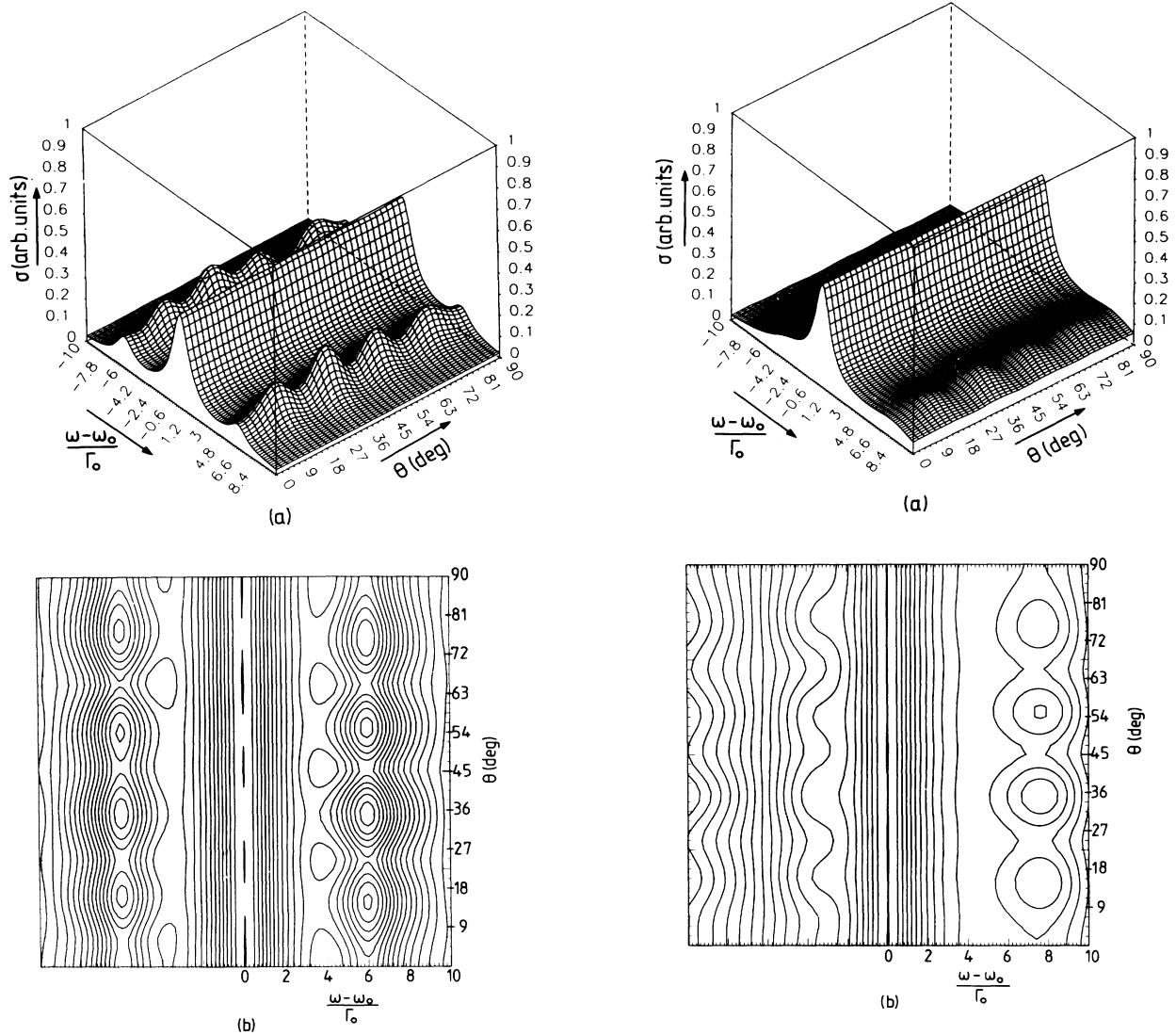


FIG. 13. Mössbauer spectra including quadrupole interaction and diffusion broadening for the parameters listed in Table II. Arrangement of plots as in Fig. 7.

FIG. 14. Mössbauer spectra showing diffusion broadening, isomer shift, and partially averaged quadrupole interaction due to slow rotation of vacancies in the NN shell of the MA (for parameters see text and Table II).

with the asymmetry caused by anisotropic vibration amplitudes of MA's.

There are two mechanisms in our model for the relaxation of the quadrupole interaction. First, the fluctuation of the magnitude due to association and dissociation jumps of vacancies just as in the case of isomer shift. Secondly, the fluctuation of the direction of the axis of the field gradient due to rotational jumps of vacancies in the NN shell of the MA. For the spectrum shown in Fig. 13 both mechanisms are ineffective because the fluctuation rates are too small. Figure 14 shows a spectrum for $\Delta = 2\Gamma_0$ and $w_1 = 0.5\Gamma_0 < Q = \Gamma_0$. The quadrupole interaction is partially averaged by the rotation jumps but

the isomer shift is unaffected since $w_3 = w_4 = 0.005\Gamma_0 \ll \Delta$. The spectrum shown in Fig. 15 is calculated with the parameters obtained¹ for the diffusion of ^{57}Fe in Al (see Table II), and in addition, assuming $\Delta = 2\Gamma_0$ and $Q = 2\Gamma_0$. As can be seen, the quadrupole interaction is completely averaged out due to the large rotational jump rate of the vacancies $w_1 = 130\Gamma_0$. On the other hand, the slight asymmetry of the spectrum shows that the isomer shift is not completely averaged due to the relatively small association and dissociation rates. However, the measured spectra are symmetric. This means that in the actual system Fe in Al the isomer shift due to a NN vacancy must be less than $2\Gamma_0$.

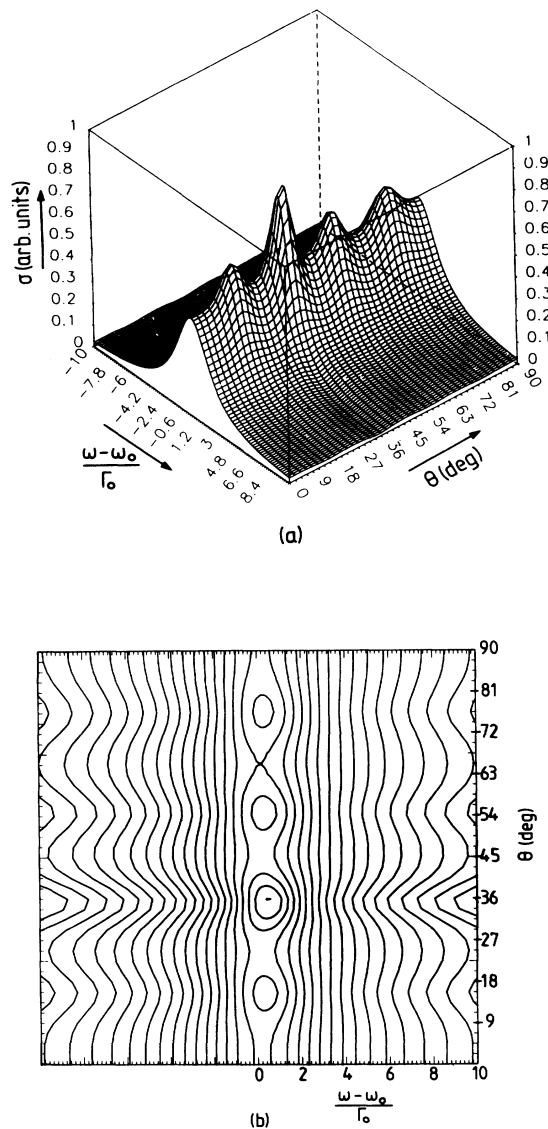


FIG. 15. Mössbauer spectra for vacancy jump frequencies obtained (Ref. 1) for diffusion in Fe in Al, in addition including isomer shift and quadrupole interaction (for parameters see Table II). Fast rotation of vacancies in the NN shell of the MA leads to complete averaging of the quadrupole interaction; averaging of the isomer shift is incomplete.

V. DISCUSSION AND CONCLUSIONS

With our model we can describe the Mössbauer emission spectrum considering the influence of diffusion of the MA and of fluctuating hyperfine interactions induced by vacancies. The results for single crystals show anisotropic diffusion broadening of the Mössbauer spectra and motional narrowing of the hyperfine interactions, depending on the magnitude of the vacancy jump frequencies involved. The anisotropy depends on the lattice structure; explicit calculations are presented for sc lattices (analyti-

cal) and fcc lattices (numerical calculations).

It turns out that in the systems investigated experimentally so far, e.g., dilute metallic alloys like Fe in Al at high temperatures,¹ the relaxation of the hyperfine interactions cannot be detected for two major reasons: (i) the vacancy concentration is too small, and (ii) hyperfine interactions of reasonable size (comparable in magnitude to the natural linewidth) will be averaged out by the relatively high vacancy jump rates. Thus we have confirmed the applicability of the analysis neglecting hyperfine interactions used to interpret experiments on diffusion broadening at high temperatures.¹ Only in systems with NN vacancy concentrations in the percent range at low temperatures (small vacancy jump rates), can all the features of the model be detected since then the intensity of the lines carrying the characteristics of the vacancy-induced hyperfine interactions is strong enough.

Such systems might be (partially) ordered nearly stoichiometric metallic alloys of $B2$ structure like Fe-Al, Pd-Si, Co-Ga, or of DO_3 structure like Cu_3Sn which contain a large concentration of structural vacancies to compensate for nonstoichiometry. The question of if and how these structural vacancies participate in atomic diffusion is still open to discussion.²⁰ Other systems with high vacancy concentration on the metallic sublattice are transition-metal oxides like FeO with oxygen excess.²¹

We suggest that measurements of the Mössbauer emission spectra in these systems at low temperatures should be made. The results could be interpreted with our theoretical model and should reveal details of the kinetics of atomic motion, in particular, if systems with large vacancy-induced hyperfine interactions are investigated.

Other nuclear methods like perturbed angular correlation (PAC),²² NMR,²³ and β -NMR,²⁴ can also be used to investigate the relaxation of vacancy-induced hyperfine interactions. However, these methods lack the direct information about jump geometry via the anisotropy of the linewidth. The theoretical treatment proceeds along similar lines as presented here for the case of the Mössbauer effect, e.g., a review can be found in Ref. 18.

Recently, the Mössbauer effect has also been applied to study the dynamics of biologically relevant protein systems like hemoglobin.²⁵⁻²⁷ The model description of the influence of the protein dynamics on the Mössbauer spectrum contains features analogous to the vacancy jumps in our model: fluctuation of the main axes of the electric field gradient responsible for the quadrupole interaction, change of the magnitude and/or symmetry of the hyperfine interactions, and displacements of the Fe atom in the complex due to change of the configuration have been considered. This suggests that our model could be adopted for the interpretation of Mössbauer emission spectra of ^{57}Fe from such systems.

ACKNOWLEDGMENTS

One of the authors (S.D.) would like to thank the Alexander von Humboldt Stiftung for support and the Institut für Festkörperforschung, Kernforschungsanlage Jülich for kind hospitality.

APPENDIX A: PURE DIFFUSIONAL EFFECTS
IN THE s_c STRUCTURE

We furnish here the steps leading to Eq. (2.26) in the text. We may recall from Eqs. (2.21) and (2.22) that our basic task is to compute the matrix elements of $\tilde{P}_k(s)$ upon inverting the matrix $(s\mathbb{1} - \underline{W}_k)$, and then evaluate the sum over α and β . This is performed by splitting the matrix \underline{W}_k into four terms and exploiting certain properties of these terms, as indicated below. Similar strategies had been employed in Ref. 15.

Using Eqs. (2.5) and (2.25) we may write from Eq. (2.24)

$$\underline{W}_k^0 = \begin{pmatrix} & 1 & -1 & 2 & -2 & 3 & -3 & N \\ 1 & -\gamma' & (w_2 e^{i\delta_1} - w_1) & 0 & 0 & 0 & 0 & 0 \\ -1 & (w_2 e^{-i\delta_1} - w_1) & -\gamma' & 0 & 0 & 0 & 0 & 0 \\ 2 & 0 & 0 & -\gamma' & (w_2 e^{i\delta_2} - w_1) & 0 & 0 & 0 \\ -2 & & & (w_2 e^{-i\delta_2} - w_1) & -\gamma' & 0 & 0 & 0 \\ 3 & 0 & 0 & 0 & 0 & -\gamma' & (w_2 e^{i\delta_3} - w_1) & 0 \\ -3 & 0 & 0 & 0 & 0 & (w_2 e^{-i\delta_3} - w_1) & -\gamma' & 0 \\ N & 0 & 0 & 0 & 0 & 0 & 0 & \gamma \end{pmatrix}. \quad (\text{A5})$$

In Eq. (A5)

$$\delta_i = \mathbf{k} \cdot \mathbf{r}_i, \quad i = 1, 2, 3 \quad (\text{A6})$$

and γ and γ' are defined in Eqs. (2.30) and (2.31). Using the operator identity:

$$\frac{1}{\underline{A}} = \frac{1}{\underline{B}} + \frac{1}{\underline{B}}(\underline{B} - \underline{A})\frac{1}{\underline{A}} = \frac{1}{\underline{B}} + \frac{1}{\underline{A}}(\underline{B} - \underline{A})\frac{1}{\underline{B}} \quad (\text{A7})$$

we may write from Eqs. (2.21) and (A1),

$$\tilde{P}_k(s) = \underline{P}' + \underline{P}'[w_1 \underline{W}_1 + (\nu - w_1) \underline{W}_2] \tilde{P}_k(s), \quad (\text{A8})$$

where

$$\underline{P}' \equiv [s - \underline{W}_k^0 - (\lambda - w_1) \underline{W}_3]^{-1}. \quad (\text{A9})$$

Note that we have not indicated the \mathbf{k} and s dependence of \underline{P}' , for the sake of brevity. Equation (A8) allows us to write

$$\begin{aligned} \sum_{\alpha, \beta} (\alpha | \tilde{P}_k(s) | \beta) p_\beta &= \sum_{\alpha, \beta} (\alpha | \underline{P}' | \beta) p_\beta \\ &+ \sum_{\alpha, \beta, \alpha', \beta'} (\alpha | \underline{P}' | \alpha') \\ &\quad \times (\alpha' | [w_1 \underline{W}_1 + (\nu - w_1) \underline{W}_2] | \beta') \\ &\quad \times (\beta' | \tilde{P}_k(s) | \beta) p_\beta, \end{aligned}$$

where in the second term on the right we have used the completeness relation:

$$\underline{W}_k = \underline{W}_k^0 + w_1 \underline{W}_1 + (\nu - w_1) \underline{W}_2 + (\lambda - w_1) \underline{W}_3, \quad (\text{A1})$$

where

$$(\alpha | \underline{W}_1 | \beta) = 1 \quad (\text{independent of } \alpha \text{ and } \beta), \quad (\text{A2})$$

$$(\alpha | \underline{W}_2 | \beta) = \delta_{\alpha N} \quad (\text{independent of } \beta), \quad (\text{A3})$$

$$(\alpha | \underline{W}_3 | \beta) = \delta_{\beta N} \quad (\text{independent of } \alpha), \quad (\text{A4})$$

and the matrix \underline{W}_k^0 is a 2×2 block matrix given by

$$\sum_{\alpha} |\alpha\rangle \langle \alpha| = 1. \quad (\text{A10})$$

Employing next the properties of the matrices \underline{W}_1 and \underline{W}_2 as given in Eqs. (A2) and (A3) we obtain

$$\begin{aligned} \sum_{\alpha, \beta} (\alpha | \tilde{P}_k(s) | \beta) p_\beta &= \sum_{\alpha, \beta} (\alpha | \underline{P}' | \beta) p_\beta \\ &+ \sum_{\alpha, \alpha'} (\alpha | \underline{P}' | \alpha') [w_1 + (\nu - w_1) \delta_{\alpha N}] \\ &\quad \times \sum_{\beta, \beta'} (\beta' | \tilde{P}_k(s) | \beta) p_\beta \end{aligned}$$

and therefore,

$$\begin{aligned} \sum_{\alpha, \beta} (\alpha | \tilde{P}_k(s) | \beta) p_\beta &= \left[1 - \left[w_1 \sum_{\alpha, \alpha'} (\alpha | \underline{P}' | \alpha') \right. \right. \\ &\quad \left. \left. + (\nu - w_1) \sum_{\alpha} (\alpha | \underline{P}' | N) \right] \right]^{-1} \sum_{\alpha, \beta} (\alpha | \underline{P}' | \beta) p_\beta. \end{aligned} \quad (\text{A11})$$

Thus the left-hand side of Eq. (A11), required in the line-shape computation [cf. Eq. (2.22)], is determined completely in terms of certain matrix elements of \underline{P}' . Our next step is to write \underline{P}' , using again the identity in Eq. (A7), as

$$\underline{P}' = \underline{P}^0 + \underline{P}'[(\lambda - w_1) \underline{W}_3] \underline{P}^0, \quad (\text{A12})$$

where [cf. Eq. (A9)],

$$\underline{P}^0 \equiv (s - \underline{W}_k^0)^{-1}. \quad (\text{A13})$$

The strategy then is to calculate the terms involving \underline{P}' in Eq. (A11) in terms of the matrix elements of \underline{P}^0 . First, note that

$$\begin{aligned} \sum_{\alpha} (\alpha | \underline{P}' | N) &= \sum_{\alpha} (\alpha | \underline{P}^0 | N) \\ &+ \sum_{\alpha, \alpha'} (\alpha | \underline{P}' | \alpha') (\lambda - w_1) (N | \underline{P}^0 | N), \end{aligned} \quad (\text{A14})$$

where we have used Eqs. (A4) and (A12). Next,

$$\begin{aligned} \sum_{\alpha, \alpha'} (\alpha | \underline{P}' | \alpha') &= \sum_{\alpha, \alpha'} (\alpha | \underline{P}^0 | \alpha') \\ &+ \sum_{\alpha, \beta, \alpha'} (\alpha | \underline{P}' | \beta) (\lambda - w_1) (N | \underline{P}^0 | \alpha') \end{aligned}$$

and therefore,

$$\begin{aligned} \sum_{\alpha, \alpha'} (\alpha | \underline{P}' | \alpha') &= \left[1 - \sum_{\beta} (\lambda - w_1) (N | \underline{P}^0 | \beta) \right]^{-1} \\ &\times \sum_{\alpha, \alpha'} (\alpha | \underline{P}^0 | \alpha'). \end{aligned} \quad (\text{A15})$$

This expression may now be substituted in Eq. (A14). Finally

$$\begin{aligned} \sum_{\alpha, \beta} (\alpha | \underline{P}' | \beta) p_{\beta} &= \sum_{\alpha, \beta} (\alpha | \underline{P}^0 | \beta) p_{\beta} \\ &+ \sum_{\alpha, \alpha'} (\alpha | \underline{P}' | \alpha') (\lambda - w_1) \\ &\times \sum_{\beta} (N | \underline{P}^0 | \beta) p_{\beta}, \end{aligned} \quad (\text{A16})$$

where the term involving \underline{P}' is given in Eq. (A15).

Thus we find that all the relevant terms in Eq. (A11) are calculable in terms of the matrix elements of \underline{P}^0 . Now, \underline{P}^0 is given by Eq. (A13) where the matrix \underline{W}_k^0 is indicated in Eq. (A5). Using the latter we evaluate below the required terms involving \underline{P}^0 . First,

$$(N | \underline{P}^0 | N) = (s - \gamma)^{-1}. \quad (\text{A17})$$

$$\sum_{\alpha, \beta} (\alpha | \tilde{\underline{P}}_k(s) | \beta) p_{\beta} = \left[\left[1 - \frac{\nu - w_1}{s - \gamma} - \frac{w_1(s - \gamma) + (\nu - w_1)(\lambda - w_1)}{s + \nu + 6\lambda} \bar{G}^0 \right]^{-1} \left[\langle G^0 \rangle + p_N \frac{\lambda - w_1}{s + \nu + 6\lambda} \bar{G}^0 \right] \right]. \quad (\text{A24})$$

Equation (A24), put together with Eq. (2.22), yields Eq. (2.26), quoted in the text.

APPENDIX B: COMBINED EFFECTS OF DIFFUSION AND HYPERFINE INTERACTION IN THE sc STRUCTURE

We provide below the derivation of Eq. (3.16). Unlike the treatment given in Appendix A the required matrix $\tilde{\underline{U}}(s, \mathbf{k})$ [cf. Eq. (3.13)] is now labeled by nuclear angular momentum indices as well, since V_j is a quantum operator. As mentioned earlier, in order to compute $\tilde{\underline{U}}(s, \mathbf{k})$ we

Second,

$$\sum_{\alpha} (N | \underline{P}^0 | \alpha) = \sum_{\alpha} (\alpha | \underline{P}^0 | N) = (N | \underline{P}^0 | N) = (s - \gamma)^{-1}. \quad (\text{A18})$$

Third,

$$\sum_{\alpha, \beta} (\alpha | \underline{P}^0 | \alpha') = \bar{G}^0 \quad (\text{A19})$$

and

$$\sum_{\alpha, \beta} (\alpha | \underline{P}^0 | \beta) p_{\beta} = \langle G^0 \rangle, \quad (\text{A20})$$

where \bar{G}^0 and $\langle G^0 \rangle$ have been defined in Eqs. (2.27) and (2.28), respectively. In computing the left-hand sides of Eqs. (A19) and (A20) we have made use of the fact that \underline{W}_k^0 can be split into block matrices [cf. Eq. (A5)], the largest being of dimension 2×2 only.

Collecting all the pieces together, we obtain [cf. (A15)]

$$\sum_{\alpha, \alpha'} (\alpha | \underline{P}' | \alpha') = \left[1 - \frac{(\lambda - w_1)}{(s - \gamma)} \right]^{-1} \bar{G}^0 = \frac{(s - \gamma)}{(s + \nu + 6\lambda)} \bar{G}^0. \quad (\text{A21})$$

Equation (A14) then yields

$$\sum_{\alpha} (\alpha' | \underline{P}' | N) = (s - \gamma)^{-1} \left[1 + \frac{(\lambda - w_1)(s - \gamma)}{(s + \nu + 6\lambda)} \bar{G}^0 \right]. \quad (\text{A22})$$

Finally, from Eq. (A16),

$$\sum_{\alpha, \beta} (\alpha | \underline{P}' | \beta) p_{\beta} = \langle G^0 \rangle + \frac{(\lambda - w_1)}{(s + \nu + 6\lambda)} \bar{G}^0 p_N, \quad (\text{A23})$$

where we have employed Eq. (A21).

Substituting Eqs. (A21)–(A23) in Eq. (A11) we arrive at

have to invert a 28×28 matrix, since there are four angular momentum indices and seven stochastic indices. However, the operations *within* only the stochastic ‘space’ can be carried out in an exactly analogous manner as in Appendix A. Thus, parallel to Eq. (A24) we now derive

$$\begin{aligned} (\tilde{\underline{U}}(s, \mathbf{k}))_{\text{av}} &= \sum_{\alpha, \beta} (\alpha | \tilde{\underline{U}}(s, \mathbf{k}) | \beta) p_{\beta} \\ &= \underline{R}^{-1} \left[\langle \underline{U}^0 \rangle + p_N \frac{\lambda - w_1}{s + \nu + 6\lambda} \underline{\bar{U}}^0 \right], \quad (\text{B1}) \\ \underline{R} &= \left[1 - \frac{\nu - w_1}{s - \gamma} - \frac{w_1(s - \gamma) + (\nu + w_1)(\lambda - w_1)}{s + \nu + 6\lambda} \underline{\bar{U}}^0 \right], \end{aligned}$$

where, however, \bar{U}^0 and $\langle U^0 \rangle$, unlike \bar{G}^0 and $\langle G^0 \rangle$, are quantum operators. They are defined by

$$\begin{aligned}\bar{U}^0 &\equiv \sum_{\alpha, \beta} (\alpha | U^0 | \beta) , \\ \langle U^0 \rangle &\equiv \sum_{\alpha, \beta} (\alpha | U^0 | \beta) p_{\beta} ,\end{aligned}\quad (\text{B2})$$

where

$$U^0 = \left[s - \underline{W}_k^0 - \frac{i}{\hbar} \sum_j V_j F_j \right]^{-1}. \quad (\text{B3})$$

Retaining the operator character of V_j and restricting attention to the stochastic space only, the matrix elements

$$U^0 = \begin{pmatrix} 1 & \frac{1}{D_1} \begin{bmatrix} (\Omega_1 + \gamma') & (w_2 e^{i\delta_1} - w_1) \\ (w_2 e^{-i\delta_1} - w_1) & (\Omega_1 + \gamma') \end{bmatrix} & 2 & -2 & 3 & -3 & N \\ -1 & \frac{1}{D_1} \begin{bmatrix} (\Omega_1 + \gamma') & (w_2 e^{i\delta_1} - w_1) \\ (w_2 e^{-i\delta_1} - w_1) & (\Omega_1 + \gamma') \end{bmatrix} & 0 & 0 & 0 & 0 & 0 \\ 2 & 0 & \frac{1}{D_2} \begin{bmatrix} (\Omega_2 + \gamma') & (w_2 e^{i\delta_2} - w_1) \\ (w_2 e^{-i\delta_2} - w_1) & (\Omega_2 + \gamma') \end{bmatrix} & 0 & 0 & 0 & 0 \\ -2 & 0 & \frac{1}{D_2} \begin{bmatrix} (\Omega_2 + \gamma') & (w_2 e^{i\delta_2} - w_1) \\ (w_2 e^{-i\delta_2} - w_1) & (\Omega_2 + \gamma') \end{bmatrix} & 0 & 0 & 0 & 0 \\ 3 & 0 & 0 & 0 & \frac{1}{D_3} \begin{bmatrix} (\Omega_3 + \gamma') & (w_2 e^{i\delta_3} w_1) \\ (w_2 e^{-i\delta_3} - w_1) & (\Omega_3 + \gamma') \end{bmatrix} & 0 & 0 \\ -3 & 0 & 0 & 0 & \frac{1}{D_3} \begin{bmatrix} (\Omega_3 + \gamma') & (w_2 e^{i\delta_3} w_1) \\ (w_2 e^{-i\delta_3} - w_1) & (\Omega_3 + \gamma') \end{bmatrix} & 0 & 0 \\ N & 0 & 0 & 0 & 0 & 0 & (s - \gamma)^{-1} \end{pmatrix}, \quad (\text{B6})$$

where

$$D_i = (\Omega_i + \gamma')^2 - (w_1^2 + w_2^2 - 2w_1 w_2 \cos \delta_i). \quad (\text{B7})$$

Using Eq. (B6) it is evident from Eq. (B2) that

$$\bar{U}^0 = 2 \sum_{i=1}^3 [\Omega_i + \nu + 4w_1 + w_2(1 + \cos \delta_i)] / D_i + (s - \gamma)^{-1} \quad (\text{B8})$$

and

$$\begin{aligned}\langle U^0 \rangle &= 2p_A \sum_{i=1}^3 [\Omega_i + \nu + 4w_1 \\ &\quad + w_2(1 - \cos \delta_i)] / D_i + p_N (s - \gamma)^{-1} .\end{aligned}\quad (\text{B9})$$

Equations (B8) and (B9) may be contrasted with Eqs. (2.27) and (2.28) in the text.

At this stage it is well to recognize that \bar{U}^0 and $\langle U^0 \rangle$ are just quantum operators which have a 4×4 matrix representation since the nuclear angular momentum is $\frac{3}{2}$ in the excited state. It is possible then to make further simplification in the analysis upon exploiting certain symmetry properties of the quadrupolar Hamiltonian in Eqs. (3.6)–(3.8) for $I = \frac{3}{2}$, as shown below.

First, note that

$$\begin{aligned}[\Omega_i + \nu + 4w_1 + w_2(1 + \cos \delta_i)] / D_i \\ = C_i^+ / (\nu + \Omega_i + A_i^+) + C_i^- / (\nu + \Omega_i + A_i^-) ,\end{aligned}\quad (\text{B10})$$

of $(U^0)^{-1}$ within that space can be in Eq. (B4) (displayed on opposite page), where

$$\begin{aligned}\Omega_1 &= s + (i/\hbar) [\Delta(I) + Q(3I_x^2 - I^2)] , \\ \Omega_2 &= s + (i/\hbar) [\Delta(I) + Q(3I_y^2 - I^2)] , \\ \Omega_3 &= s + (i/\hbar) [\Delta(I) + Q(3I_z^2 - I^2)] .\end{aligned}\quad (\text{B5})$$

Although Ω_1 , Ω_2 , and Ω_3 are noncommuting operators they may be treated as C numbers as far as manipulations of the matrix in Eq. (B4) are concerned in view of its special block nature. Thus

where A_i^\pm and C_i^\pm have been defined earlier in Eq. (2.39). Next, we may decompose either term in the right-hand side of Eq. (B10) as

$$C_i^\pm / (\nu + \Omega_i + A_i^\pm) = C_i^\pm / (q_i^\pm + V_i) , \quad (\text{B11})$$

where q_i^\pm have been defined in Eq. (3.18) and

$$V_i = Q(3I_i^2 - I^2), \quad i = x, y, z . \quad (\text{B12})$$

Observe now the interesting property that

$$V_i^2 = 9Q^2 \quad (\text{B13})$$

for $I = \frac{3}{2}$. This permits us to simplify Eq. (B11) by a direct power series expansion, as

$$\begin{aligned}C_i^\pm / (\nu + \Omega_i + A_i^\pm) \\ = C_i^\pm (q_i^\pm - (i/\hbar)V_i) / ((q_i^\pm)^2 + 9(Q/\hbar)^2) .\end{aligned}\quad (\text{B14})$$

Therefore, the matrix elements of \bar{U}^0 and $\langle U^0 \rangle$ can be simply read off from the known matrix elements of V_i , which are listed below. Using the properties of angular momentum operators,²⁸ we have

$$V_x = \frac{3}{2} 3Q \begin{pmatrix} \frac{3}{2} & \frac{1}{2} & -\frac{1}{2} & -\frac{3}{2} \\ -\frac{1}{2} & 0 & \sqrt{3}/2 & 0 \\ \frac{1}{2} & \frac{1}{2} & 0 & \sqrt{3}/2 \\ -\frac{3}{2} & \sqrt{3}/2 & \frac{1}{2} & 0 \\ 0 & \sqrt{3}/2 & 0 & -\frac{1}{2} \end{pmatrix} ,$$

- Litterst, A. M. Afanas'ev, P. Alexandrov, and V. Gorobtschenko, *Solid State Commun.* **45**, 963 (1983); F. J. Litterst, V. D. Gorobtschenko, and G. M. Kalvius, *Hyperfine Interact.* **14**, 21 (1983).
- ¹²M. Blume, *Phys. Rev.* **174**, 351 (1968).
- ¹³See, for example, G. Vogl, W. Mansel, and P. H. Dederichs, *Phys. Rev. Lett.* **36**, 1497 (1976); see also T. Springer, *Diffusion and Rotational Motion*, Vol. 3 of *Topics in Current Physics* edited by S. W. Lovesey, T. Springer, R. Comès (Springer, Berlin, Heidelberg, New York, 1977).
- ¹⁴See, for example, S. Dattagupta and M. Blume, *Phys. Rev. B* **10**, 4540 (1974).
- ¹⁵S. Dattagupta, *Philos. Mag.* **33**, 59 (1976).
- ¹⁶J. A. Tjon and M. Blume, *Phys. Rev.* **165**, 456 (1968).
- ¹⁷K. Schroeder, D. Wolf, and P. H. Dederichs, in *Point Defects and Defect Interactions in Metals*, edited by J. I. Takamura, M. Doyama, and M. Kiritani (University of Tokyo, Tokyo, 1982), p. 570.
- ¹⁸S. Dattagupta, *Hyperfine Interact.* **11**, 77 (1981).
- ¹⁹V. I. Goldanskii and E. F. Makarov, in *Chemical Applications of Mössbauer Spectroscopy*, edited by V. I. Goldanskii and R. H. Herber (Academic, New York, 1968), p. 102.
- ²⁰G. Froberg and H. Wever, in *Point Defects and Defect Interactions in Metals*, Ref. 17, p. 614.
- ²¹C. P. Flynn, *Point Defects And Diffusion* (Clarendon Press, Oxford, 1972), p. 67.
- ²²E. Recknagel, G. Schatz, and Th. Wichert, in *Hyperfine Interactions of Radioactive Nuclei*, Vol. 31 of *Topics in Current Physics*, edited by J. Christiansen (Springer, Berlin, Heidelberg, New York, 1982); E. Recknagel and Th. Wichert, *Nucl. Instr. Methods* **182/183**, 439 (1981).
- ²³C. Minier and M. Minier, in *Point Defects and Defect Interactions in Metals*, Ref. 17, p. 27.
- ²⁴P. Heitjans, *Solid State Ionics* **18/19**, 50 (1986).
- ²⁵H. Keller and P. G. Debrunner, *Phys. Rev. Lett.* **45**, 68 (1980).
- ²⁶I. Nowik, S. G. Cohen, E. R. Bauminger, and S. Ofer, *Phys. Rev. Lett.* **50**, 1528 (1983).
- ²⁷L. W. Knapp, S. F. Fischer, and F. Parak, *J. Chem. Phys.* **78**, 4701 (1983).
- ²⁸A. Messiah, *Quantum Mechanics* (North-Holland, Amsterdam, 1965), Vol. 2, Chap. VIII.